Applied Thermal Engineering 214 (2022) 118736

Contents lists available at ScienceDirect

Applied Thermal Engineering

journal homepage: www.elsevier.com/locate/apthermeng

Research Paper

Performance enhancement of horizontal extension and thermal energy storage to an abandoned exploitation well and satellite LNG station integrated ORC system

Fei Xiao [a,b], Lizhong Yang [b,c,*], Lei He [d], Antoni Gil [b], Srithar Rajoo [e], Zhiye Zhao [f], Alessandro Romagnoli [g], Luisa F. Cabeza [c]

[a] Department of Civil Engineering, Nanjing University of Aeronautics and Astronautics, Nanjing, 210016, China
[b] Surbana Jurong – Nanyang Technological University Corporate Lab, 61 Nanyang Drive, 637355, Singapore
[c] GREiA Research Group, Universitat de Lleida, Pere de Cabrera s/n, 25001 Lleida, Spain
[d] School of Civil Engineering, Southeast University, Nanjing 211189, China
[e] Faculty of Mechanical Engineering, Universiti Teknologi Malaysia (UTM), Johor, Malaysia
[f] School of Civil and Environmental Engineering, Nanyang Technological University, 50 Nanyang Avenue, 639798, Singapore
[g] School of Mechanical and Aerospace Engineering, Nanyang Technological University, 50 Nanyang Avenue, 639798, Singapore

ARTICLE INFO

Keywords:
Abandoned Exploitation Well (AEW)
LNG cold energy
Geothermal
Thermal energy storage
Organic Rankine Cycle (ORC)
Off-design operation

ABSTRACT

Tens of millions of abandoned exploitation wells (AEW) exist throughout the world, posing a threat to the environment and costing extra investment for decommissioning. Revitalization of the AEW offers a cost-effective solution for geothermal energy exploitation by saving the high costs of decommissioning and drilling. However, the thermal resources from AEW are usually of low and medium grade. Measures should be taken to increase the efficiency of AEW geothermal power plants. Meanwhile, the regasification process of satellite liquified natural gas (LNG) stations worldwide suffer from a loss of high-grade cold energy. Various studies have used geothermal heat and LNG cold to produce electricity, yet the horizontal extension of the AEW that may increase the recovered temperature, and the fluctuation of the LNG flow that may reduce the power output, were not discussed. This study proposes and evaluates a novel integrated organic Rankine cycle (ORC) system that uses the geothermal heat from the AEWs and waste LNG cold energy from satellite LNG stations, focusing on the performance enhancement of horizontal extension to increase the geothermal temperature and thermal energy storage to stabilize the LNG cold energy supply. A numerical model is developed that considers the horizontal extension in the AEW, and the horizontal extension is found to significantly increase the geothermal fluid temperature. A machine learning-based predictive model is built to assess the AEW outlet temperature under given parameters and working conditions. Cold thermal energy storage (CTES) modules are designed and optimized to stabilize the waste cold energy recovery when exposed to highly fluctuating LNG supply during off-design operation. CTES increased the ORC efficiency by 38.5% and has the potential to significantly shorten the payback period. Therefore, by utilizing the horizontal extension of the AEW and combining the power generation with LNG cold through thermal energy storage, the zero-emission geothermal and waste cold energy-based system can be a viable solution for future AEW revitalization and LNG waste cold energy utilization.

1. Introduction

While the world is rapidly switching to cleaner energy sources such as wind, solar, hydropower, and geothermal, we still have to deal with the aftermath of centuries of oil and gas exploration and production. Around 29 million exploitation wells are estimated to have been left over globally, and the number is still snowballing [43,31]. If not properly treated, the abandoned exploitation wells (AEWs) can lead to groundwater pollution, methane emissions, and contamination of the surface environment [13,26,5,49]. However, as shown in Table 1, extra financial investment is required for the further treatment of the AEWs. Several other researchers also discussed the abandonment cost of onshore wells [46]. It was reported that the cost of onshore well

* Corresponding author.
E-mail address: lzyang@ntu.edu.sg (L. Yang).

https://doi.org/10.1016/j.applthermaleng.2022.118736
Received 3 March 2022; Received in revised form 16 May 2022; Accepted 24 May 2022
Available online 27 May 2022

Nomenclature

Acronyms

AEW	Abandoned exploitation well
BHE	Borehole heat exchanger
CAPEX	Capital expenditure
CEPCI	Chemical engineering plant cost index
CTES	Cold thermal energy storage
DR	Demand Response
GWP	Global warming potential
HTES	Hot thermal energy storage
HTF	Heat transfer fluid
LCOE	Levelized cost of electricity
PBP	Payback period
PCM	Phase change material
ODP	Ozone depletion potential
OPEX	Operating expense
ORC	Organic Rankine Cycle
TES	Thermal energy storage

Subscripts

B	Bottoming cycle
cold	Cold energy
cas	Casing layer
cem	Cemented layer
ci	Inner side of casing
co	Outer side of casing
D	Dimensionless
DP	Design point
ele	Electrical energy
f	Fluid
h	Horizontal
i	Inside
ins	Insulation layer
L	Length
M	Material
m	Mass
me	Electromechanical
mo	Motor
o	Outside
oi	Between outlet and inlet fluid
ti	Inner side of inside tubing
to	Inner side of outside tubing
tub	Tubing
s	Formation solid
si	Between inlet fluid and solid formation
T	Topping cycle
w	Wall
v	Vertical

Symbols

A	Area (m^2)
C	Investment cost (USD_{2020})
c_p	Specific heat capacity ($J\ kg^{-1}\ K^{-1}$)
d	Depth or distance (m)
F	Correction factor (-)
f	Friction factor (-)
h	Specific enthalpy ($J\ kg^{-1}$)
i	Discount rate (-)
L	Latent heat of fusion ($J\ kg^{-1}$)
Nu	Nusselt number (-)
$\dot{m}$	Mass flow rate ($kg\ s^{-1}$)
n	Lifetime (y)
P	Power (kW)
p	Pressure (Pa)
$\dot{Q}$	Heat flow rate (W)
q	Heat flow ($W\ m^{-2}$)
r	Radius of structure component (m)
R	Thermal resistance ($m^2\ K\ W^{-1}$)
s	Specific entropy ($J\ kg^{-1}\ K^{-1}$)
SIC	Specific investment cost ($USD_{2020}\ kW^{-1}$)
T	Temperature (K)
t	Time (s or y)
U	Coefficient of heat transfer ($W\ m^2\ K^{-1}$)
u	Dummy variable for integration (-)
v	Velocity ($m\ s^{-1}$)
$\dot{W}$	Work (W)
x	Downward length along the AEW axis (m)

Greek symbols

α	Thermal diffusivity ($m^2\ s^{-1}$)
β	Share of the other costs in a conventional geothermal plant (-)
Δ	Equivalent absolute roughness (m)
ΔT_{PC}	Phase transition range (K)
δ	Thickness (m)
η	Efficiency (-)
λ	Thermal conductivity ($W\ m^{-1}\ K^{-1}$)
μ	Dynamic viscosity (Pa s)
ρ	Density ($kg\ m^{-3}$)
τ_f	Friction loss gradient of pressure ($Pa\ m^{-1}$)
ω	Ratio of volumetric heat capacity (-)

abandonment in New Brunswick, Canada, ranged from CAD 22,860 to CAD 16,470, considering the different well depths and other scenarios [50]. The abandonment of wells located in Block "R" Central Sumatra Basin can cost up to USD 76,000 in 2015, while the cost can be reduced year by year to USD 52,000 in 2017 if optimization is introduced [59]. As for the abandonment of wells in Block "G" in South Sumatra, the associated cost was estimated to fall between USD 60,000 to USD 1,500,000 [59]. Ojukwu reported that the well abandonment cost in Nigeria can be approximately one million dollars per well excluding the even higher costs due to facility decommissioning and removal, field restoration, and site reclamation [57]. In 2010, Kant presented the cost breakdown of well abandonment in Schoonebeek oil field in the Netherland [45], as listed in Table 2.

Therefore, instead of directly decommissioning the AEWs, increasing attention has been paid recently to utilizing the AEWs with a lower cost for consistent long-term returns, especially converting AEWs into borehole heat exchangers (BHE) to harvest the geothermal energy [25,13,19]. With the geothermal fluid circulating in a closed-loop system inside the wellbore structure with coaxial pipes to avoid fluid interaction with the surrounding formation, the risk of environmental pollution during normal operation can be minimized [20,21,24]. Furthermore, compared to conventional geothermal plants, the high cost of well drilling can be saved, which can account for up to 50% of the investment cost of a geothermal project [13].

The AEW-based geothermal sources, however, are usually of low and medium quality, with the temperature recovered less than 150℃. Hence, directly using the AEW geothermal energy for electrical power generation will result in a low efficiency due to the small temperature difference between the heat source (geothermal energy) and the cold sink (ambient environment). Some research explored using organic Rankine cycles (ORC) for AEW power generation [89,70]. For instance, Yang et al. [89] tested the 15-hour performance of a single-stage ORC

Table 1
Decommissioning costs plugging AEWs and site remediation in the US [62].

Items	States				Total
	MT	NM	PA	TX	
No. of contracts	unknown	158	103	448	913 #
No. of wells	204	158	717	448	1,527
avg wells per contract	unknown	1	7.0	1	unknown
Mean cost per well ($2019)	15,335	171,652	48,703	75,307	75,579
med ($)	9,504	132,319	24,065	58,525	52,629
mini ($)	266	8,043	3,832	1,859	266
max ($)	222,275	1,115,711	469,274	1,645,103	1,645,103
10th percentile cost * ($)	2,507	71,677	5,730	22,373	7,620
90th percentile cost * ($)	27,583	307,178	124,292	130,481	159,764
avg depth	2,409	5,987	2,056	4,226	3,880
avg first year	1959	1988	1963	1976	1973
avg plug year	2007	2016	2002	2016	2013
Share vertical or unknown	100%	93%	99%	100%	99%

Notes:
1. avg, med, mini, and max are short for average, median, minimum, and maximum cost,
2. MT, NM, PA, TX, are short for Montana, New Mexico, Pennsylvania, Texas, respectively,
3. The last column, "Total" means that count and analyze the data from all four states together,
* 10th or 90th percentile cost represents that 10% or 90% of the cost is less than this value,
# The total number of wells was specified by the regulators of Montana, while that of contracts was not specified, which could be not smaller than 913.

Table 2
Cost breakdown of activities for onshore well abandonment in Schoonebeek, the Netherland [45,46].

Category	Subclass	Average cost (USD_{2010})	Subtotal (USD_{2010})
Sub surface abandonment	Light drilling rig (per well)	100,000.00	1,340,000.00
	Heavy drilling rig (per well)	430,000.00	
	Second time by leakage of the well (per well)	810,000.00	
Environmental investigation (including plan and permit)	Well site	10,000.00	905,500.00
	Metering station	175,000.00	
	Crude oil handling	700,000.00	
	Environmental oversight (per well site)	17,000.00	
	Laboratory analysis (per well site)	3,500.00	
Surface abandonment	Clean up hardware (per well site)	17,500.00	≫ 67,500.00
	Combination Casing-Kelly (per well)	15,000.00	
	Cable removal (per meter)	7.50	
	Pipeline removal, including inside (per meter)	15.00	
	Contaminated soil (light) removal (per ton)	17.50	
	Contaminated soil (strong) removal (per ton)	45.00	
	Contaminated ground water removal (per m^3)	4.00	
	Location road removal (per meter)	175.00	
	Recultivation (per well site)	35,000.00	

system using geothermal energy extracted from an abandoned oil well in the Huabei oilfield of China. With a designed geothermal water of 85.7 °C, the efficiency of the ORC is only around 5%. Therefore, to make direct power generation a practical solution for AEW geothermal energy utilization, the temperature difference between the heat source and the cold sink temperature should be significantly increased.

One way to increase the recovered temperature from the AEW geothermal resources is to make full use of the possible horizontal extension of the exploitation wells. Traditional oil and gas exploitation wells usually consist of only a vertical wellbore. Starting from the 1980s, wells with horizontal extensions are gaining popularity, as they can hit the reservoir stratum with a higher probability and thus enhancing the associated oil or gas production [66,7,72,42,83,65]. Since the horizontal extension starts from the end of the vertical part (as shown in Fig. 1b), where the formation temperature is higher than the other parts of the well, it can increase the recovered fluid temperature for heat extraction of the AEWs. However, horizontal extension rarely appears in existing numerical models for AEW-based geothermal systems. Meanwhile, with decades of operation and abandonment, the wellbore cement layer can encounter degradation in thermal conductivity, which could affect the overall heat extraction capability of the wellbore system. Therefore, in the numerical modeling work of this study, we propose to account for the impact of the horizontal extension and the cement layer thermal conductivity on the recovered fluid temperature from the AEWs. Hence, suggestions can be given to fully utilize the horizontal extension if it exists, or the cemented layer can be revitalized if the existing layer significantly weakens the associated heat extraction capability.

For the cold sink temperature reduction, one option is to introduce a free-of-charge cold source with a lower temperature. In recent years, liquefied natural gas (LNG) has been proposed as the cold sink for conventional geothermal projects with larger scales and higher recovery temperatures than the AEWs. Among them, ORC is the most studied power cycle. Mosaffa et al. [54] compared the performance of four ORC configurations for electrical power production from geothermal heat and the waste cold energy from LNG, and found that the two-stage cascaded ORC system has the highest net power output. Similarly, Emadi and Mahmoudimehr [90] and Mehrenjani et al. [53] combined the two-stage cascaded ORC with a Proton Exchange Membrane (PEM) electrolyzer to produce cooling, power, and hydrogen. Using two geothermal wells with different temperatures and pressures, Mehdikhani et al. [52] proposed an ORC and PEM integrated system to produce power, natural gas, and hydrogen. Besides ORC, other power cycles are also discussed in the literature. Wang et al. [80] designed a transcritical CO_2 cycle using geothermal heat and LNG waste cold for electrical power production. Chen et al. [16] explored cascaded recovery of LNG cold energy with power generation cycles using CO_2 and N_2 as the working fluids. Ansarinasab et al. [80] used Kalina cycle and Stirling engine to generate pure water, cooling, heating, and electrical power. In these studies, the impacts on the system performance from the operating parameters were also investigated, such as the inlet pressure, temperature, flow rate of circulation fluids, condensing temperature of the working fluid, and temperature difference between fluids.

Compared to conventional geothermal plants with higher temperatures (usually above 150℃), LNG waste cold energy can make a more significant contribution to an AEW-based geothermal plant due to the lower-grade geothermal energy. However, few studies have investigated the synergy between AEW geothermal energy and LNG cold energy. While most AEW locations are inland and far away from primary LNG terminals located in coastal areas, many are close to residential and commercial areas [56,55], as illustrated in Fig. 1a. Therefore, it is possible to make use of the waste cold energy from the satellite LNG stations that may be collocated in the same community for AEW

(a) Above ground portion

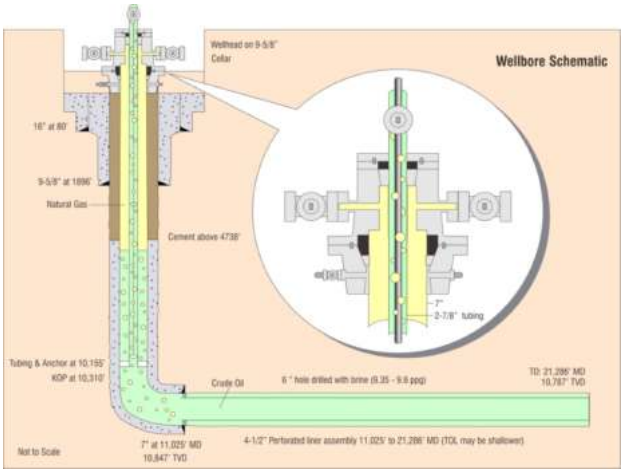

(b) Underground portion

Fig. 1. (a) above-ground structure of an oil well (in operation) close to residential and commercial areas (photo courtesy of Dr. Baichang Wang, PetroChina Company Limited), and (b) schematic diagram of the underground structure for oil exploitation [47].

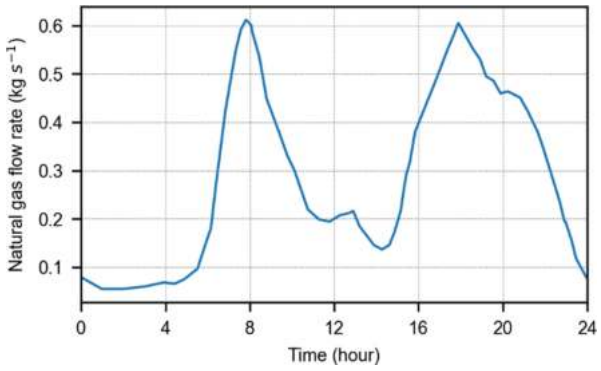

Fig. 2. A typical natural gas demand profile at a supply point in the UK (calculated based on the data from Acha et al. [3].

geothermal power production.

Satellite LNG stations are established worldwide on the customers' sites where restrictions of infrastructure, emission reduction policies, or more competitive natural gas transportation prices apply [77]. In the US, satellite stations serve as peak shaving solutions for areas with gas network restrictions or deficient storage capacity; in China, the domestic gas demand is booming so fast that trucks are delivering LNG to satellite stations nationwide before pipeline construction accomplishes; emission reduction policies also stimulate the construction of new satellite stations in the US and China; in Indonesia, Iraq, and Nigeria, satellite stations are welcomed due to high flaring levels and restrictions on power supply and transmission [77]. Transporting LNG by truck may also be economically viable in certain areas. According to the International Gas Union, truck distribution of LNG is cost-effective up to 2,000 km from the LNG terminal [27]. Meanwhile, a sizable proportion of satellite LNG stations have been built or are planned in residential and commercial areas of oil and gas production regions [8], where a large and growing number of AEWs are scattered. After receiving the LNG transported by truck tankers, the satellite stations regasify the LNG and supply them to the local natural gas grid to meet the demand of the users nearby, with a large amount of cold energy (around 830 kJ kg^{-1}) wasted. If combined with the geothermal heat from the collocated AEWs, the LNG cold energy can significantly increase the efficiency of AEW geothermal power production.

Therefore, the concept of a collocated power plant, such as an ORC cycle, is worth investigating using the geothermal heat extracted from revitalized AEWs as the heat source and the waste cold energy from the satellite LNG stations as the cold sink. Both the heat and cold sources are carbon–neutral and untapped or wasted if not being recovered for power generation. Hence, they are free-of-charge and can reduce the operational and investment costs of the AEW-based power plant, which is suitable for the nearby users and can act as a standalone power source for microgrids or a peak power plant for the utility grid.

Moreover, few studies on the use of ORCs to recover geothermal energy and LNG waste cold energy evaluated the volatility and intermittency of the LNG demand profile for LNG terminals of all sizes [32,53]. As shown in Fig. 2, the natural gas demand of a community can deviate significantly from the design point, sometimes even close to zero [3,84]. Since meeting the natural gas demand is the top priority of an LNG terminal, the high fluctuation of the input cold energy from the LNG will make the ORC system unable to meet the electricity demand and cause a significant decrease in the system efficiency and power output during off-design operation. For example, an air separation unit that relies on the LNG cold energy in Ningbo, China, can only make use of 3/4 of the available LNG cold energy due to the high fluctuation [35]. A similar intermittency or fluctuation situation can also happen to the geothermal sources if the other users (e.g., district heating) have higher priorities than the ORC [35,36]. Therefore, the problem of high fluctuation of the thermal energy supply, which is rarely discussed in the literature, should be addressed during the design phase of the AEW-ORC system. In this study, we propose a viable solution to introduce a cold thermal energy storage (CTES) and a hot thermal energy storage (HTES) system between the ORC and its cold sink and heat source. The TES systems store the surplus cold and hot energy and then discharge them during the deficit periods. Therefore, they can maintain a constant thermal power output regardless of the intermittency or fluctuation of the thermal power input. Combined with the ORC, they can provide the following benefits:

- Increase the power output of the ORC. The TES can capture most of the cold and heat supplied to the integrated system and help deliver the energy at a constant rate. Therefore, the ORC system will operate with high efficiency and make more use of the thermal energy supplied.
- Separate the thermal energy extraction and utilization processes. With the TES, the demand of each cold/heat user, such as district cooling/heating and industrial cooling/heating, can be addressed independently from each other. Hence, the TES systems can solve the mismatch between the heating, cooling, natural gas, and electricity demands.
- Increase the lifetime and reduce the maintenance cost of the ORC. By allowing the ORC to operate under constant working conditions, the

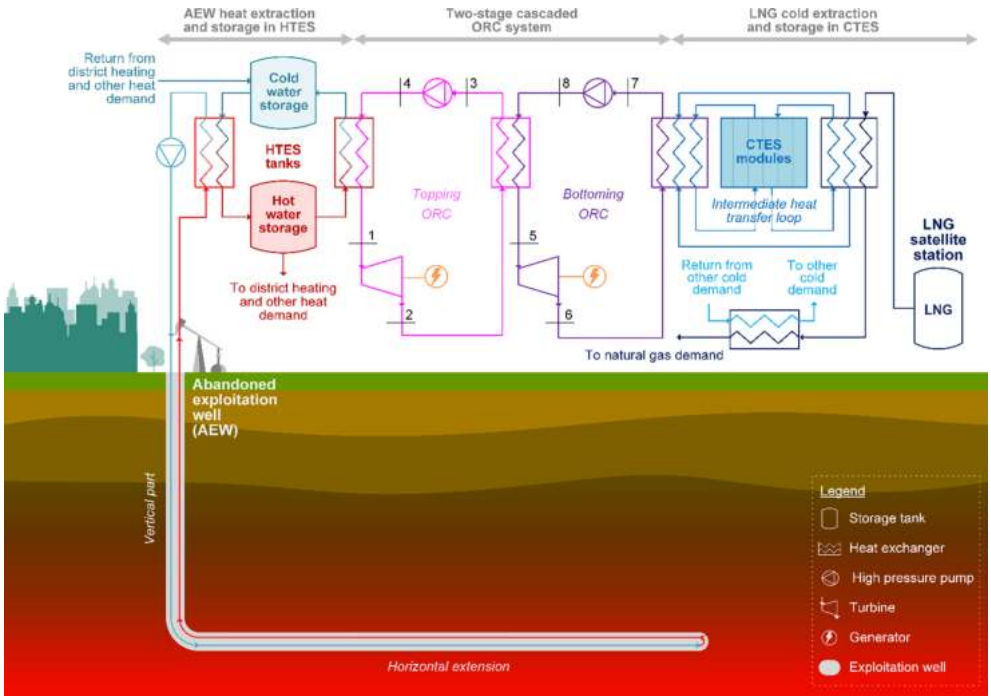

Fig. 3. Schematic of the integrated AEW-ORC power generation system. The numbers 1 to 8 are in accordance with the points in Fig. 5.

equipment lifetime can be extended. Moreover, in the extreme cases when the AEW or the LNG system leaks, severe consequences can be caused. Liquid contaminants (such as water and oil) may cause droplet erosion in the turbine and heat transfer degradation in the heat exchangers, while gaseous contaminants (such as methane) can change the composition of the working fluids in the ORC and decrease its efficiency. The TES systems can separate the cold and heat extraction with the power generation cycle, protecting the ORC system's components and reducing the frequency of working fluid replacement.

- Increase the revenue of the power generation. The TES enables the system to generate electricity during specific periods when the electricity tariff is higher, making it possible to use the whole AEW-ORC plant as a peak load shifting plant.

In summary, to improve the performance of direct power generation from AEW geothermal energy, this study proposes a novel concept of integrated ORC system with AEW horizontal extension and TES systems (Fig. 3). The geothermal energy extracted from the AEW with the horizontal extension and the waste cold energy from the satellite LNG station is stored and used as the heat source and cold sink of a cascaded ORC system. The novelties of the system design and the analysis conducted in this study are:

- Combined the waste cold energy from the collocated satellite LNG terminal to utilize the low-grade heat from AEWs to generate electricity.
- Analyzed the benefits of using the horizontal extension in the well heat exchanger model to extract higher grade heat.
- Analyzed the influence of various well parameters and working conditions on the geothermal fluid outlet temperature and ORC efficiency.
- Designed a CTES system for the varying LNG energy supply profiles and demonstrated CTES can increase the off-design power production and efficiency.

In Section 2, the integrated power generation system's transient numerical and thermodynamics models are developed to design and evaluate the heat and cold energy extraction, storage, and electrical power generation processes. Methodologies related to the techno-economic analysis are also introduced. In Section 3, the numerical and thermodynamics models are validated and then applied to case studies to analyze the factors affecting the heat extraction capacity and the performance of the integrated system during off-design operations. The role of CTES is discussed, the levelized cost of electricity (LCOE) and payback period of the system are analyzed, and recommendations are given on the application of the current system.

2. Methodology

2.1. System configuration

As illustrated in Fig. 3, the integrated ORC-geothermal-LNG power generation system mainly consists of three sectors: the AEW heat extraction and storage (left part of Fig. 3), the LNG cold energy extraction (right part of Fig. 3), and the two-stage cascaded ORC system (middle part of Fig. 3).

The geothermal energy is extracted from the AEW by converting the well to a BHE. The horizontal extension is employed to increase the temperature of the geothermal fluid. The extracted geothermal energy is stored in the dual-tank HTES system and supplied to the ORC and other heat demands such as district heating.

The LNG in the satellite station is regasified in the heat exchanger of the intermediate heat transfer loop before being supplied to the gas grid. The high-grade cold energy (lower temperature, mainly from the heat of evaporation) is supplied to the ORC or captured by the modularized CTES system. The rest of the low-grade cold energy (higher temperature, mainly from the sensible heat of the gaseous phase) is supplied to other cold demands.

A two-stage cascading ORC system (as shown in Fig. 3 and Fig. 5) is adopted to convert the heat and cold energy to electricity. Geothermal heat from the AEW is supplied to the topping cycle through the topping cycle evaporator. The LNG cold energy is delivered to the system via the bottoming cycle condenser. The heat exchanger between the two cycles acts as the evaporator of the bottoming cycle and the condenser of the topping cycle. Power generated from the topping and bottoming cycles

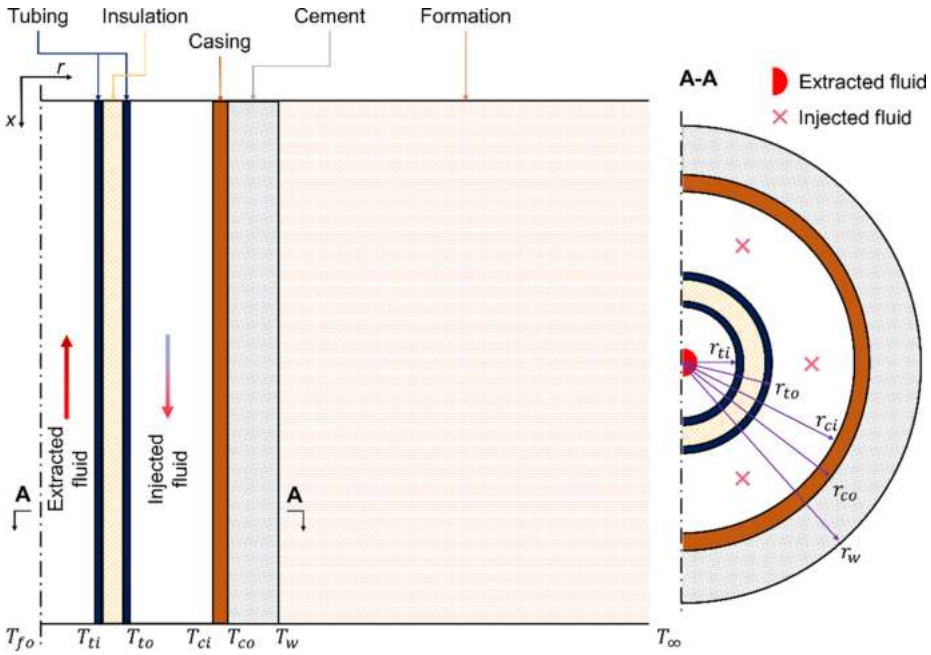

Fig. 4. Schematic diagram of AEW based borehole heat exchanger: temperature distribution and structure configuration (drawing not to scale).

are supplied to the users nearby or the electricity grid.

Details of the modeling and design methodologies for the three sectors are introduced in the following subsections. Except for the numerical model developed for the horizontal extension, all models used in this study are proven models from the literature to ensure that the results are reliable.

2.2. AEW heat extraction and storage in HTES

An AEW is usually a vertical wellbore (probably with horizontal extension, referring to Fig. 1) with a depth ranging from hundreds to thousands of meters, where the bottom hole temperature could be of an attractive value. After revitalization, an AEW can be converted to a BHE, as illustrated in Fig. 4, where there are coaxial pipes installed inside with cold fluid flowing downward through the annulus, extracting heat from the formation, while the hot fluid is moving upward through fully insulated inner tubing.

2.2.1. Assessment of the geothermal power

To assess the capacity of the BHE demonstrated in Fig. 4, it is essential to evaluate the total power P_{total} and net power P_{net} that can be generated by the system. The former can be expressed as follows [82],

$$P_{\text{total}} = q_{\text{m}}(h_{\text{o}} - h_{\text{i}})\eta_{\text{ORC}} \tag{1}$$

where q_{m} is the fluid mass flow rate; h_{o} and h_{i} are the specific enthalpies of fluid at outlet and inlet, respectively; η_{ORC} is the overall efficiency of the ORC system.

The net power is given as [82],

$$P_{\text{net}} = P_{\text{total}} - P_{\text{pump}} = P_{\text{total}} - \left(h_{\text{p1}} - h_{\text{p0}}\right)/\eta_{\text{pump}} \tag{2}$$

where P_{pump} is power consumed by the geothermal fluid feed pump; h_{p0} and h_{p1} are the specific enthalpies of fluid before and after going through the pressure pump, respectively; η_{pump} is the efficiency of pressure pump.

Nevertheless, the enthalpies in Eqs. (1) and (2) are functions of fluid pressure and temperature, which are determined by fluid dynamics and heat transfer associated with BHE and the formation.

2.2.2. Position dependent temperature

The existence of thermal resistance of formation for heat transfer leads to a temperature gradient ∇T, so the formation temperature along the wellbore axis can be expressed as,

$$T_\infty(x) = T_0 + \nabla T x, (0 \le x \le L_v) \tag{3}$$

where T_0 is the earth's surface temperature; x is the coordinate along the axis of the wellbore downward. In the present work, the wellbore is assumed to be L-shaped, the length of which in vertical and horizontal directions are L_{v} and L_{h}, respectively, with the total length $L_{\text{total}} = L_{\text{v}} + L_{\text{h}}$. Then the formation temperature around the horizontal extension can be expressed as $T_\infty(x)\,|_{(L_{\text{v}} \le x \le L_{\text{total}})} = T_0 + \nabla T L_{\text{v}}$. At the initial time $t = 0$, the temperature at the internal wall of the casing T_{ci} is T_∞.

2.2.3. Momentum equation of the fluid flow

The location-dependent fluid pressure p can be obtained via the momentum equation [17],

$$\frac{\mathrm{d}p}{\mathrm{d}x} = \rho_{\text{f}} g - \tau_{\text{f}} - \rho_{\text{f}} v_{\text{f}} \frac{\mathrm{d}v_{\text{f}}}{\mathrm{d}x} \tag{4}$$

where ρ_{f} and v_{f} are the fluid density and velocity; τ_{f} is the friction loss gradient given as [17],

$$\tau_{\text{f}} = \frac{f \rho_{\text{f}} v_{\text{f}}^2}{2 d_{\text{hydraulic}}} \tag{5}$$

where $d_{\text{hydraulic}} = 2(r_{\text{ci}} - r_{\text{to}})$ is the hydraulic diameter of the injection annulus; f is the friction factor given as [33],

$$\frac{1}{\sqrt{f}} = -1.8 \log_{10}\left[\left(\frac{\Delta / d_{\text{hydraulic}}}{3.7}\right)^{1.11} + \frac{6.9}{Re}\right] \tag{6}$$

where Δ is the equivalent absolute roughness of structure wall; $\text{Re} = \rho_{\text{f}} v_{\text{f}} d_{\text{hydraulic}} / \mu_{\text{f}}$ is Reynold's number with μ_{f} the dynamic viscosity.

2.2.4. Conductive heat transfer in the formation

For the rock formation, heat conduction is the dominant form of heat transfer. Therefore, the rate of heat transfer from the formation via the external surface of the casing within a finite distance dx can be calcu-

lated as [63],

$$d\dot{Q}_{si} = \frac{2\pi\lambda_s(T_\infty - T_w)}{\varnothing(t)}dx \tag{7}$$

where $d\dot{Q}$ is heat flow rate over dx; λ_s is the formation thermal conductivity; T_w is the temperature at the external wall of the cement layer; $\varnothing(t)$ is the function for considering transient heat conduction.

After accounting for the impact from compositive heat capacity of wellbore structure (including casing and cement layer), $\varnothing(t)$ can be expressed as [63],

$$\varnothing(t) = 16\left(\frac{\omega}{\pi}\right)^2 \int_0^\infty \frac{1 - exp(-t_D u^2)}{u^3 \Delta(u,\omega)}du \tag{8}$$

where $\omega = (\rho c_p)_s/(\rho c_p)_w$ is the ratio of volumetric heat capacity between the formation $(\rho c_p)_s$ and wellbore $(\rho c_p)_w$; $t_D = \alpha_s t/r_{ci}$ represents dimensionless time, where t is operation time, α_s is formation thermal diffusivity, and r_{ci} is the internal radius of casing layer; u is dummy variable for integration, and the complete form of $\Delta(u,\omega)$ is as follows [18],

$$\Delta(u,\omega) = [uY_0(u) - \omega Y_1(u)]^2 + [uJ_0(u) - \omega J_1(u)]^2 \tag{9}$$

where J_0 and J_1 are the zero-order and first-order Bessel function of the first kind, respectively; Y_0 and Y_1 are the zero-order and first-order Bessel function of the second kind, respectively.

2.2.5. Convective heat transfer in the circulation fluid

For the fluid flowing downwards the annulus, the temperature of which is lower than that of hot fluid flowing upward and that of the adjacent formation, so there would be heat ingress from the formation $d\dot{Q}_{si}$ and the hot fluid $d\dot{Q}_{fo}$, which can be expressed as follows,

$$d\dot{Q}_{si} = \left[2\pi r_w U_{si}(T_w - T_{fi})\right]dx \tag{10}$$

$$d\dot{Q}_{oi} = \left[2\pi r_{to} U_{oi}(T_{fo} - T_{fi})\right]dx \tag{11}$$

where r_w and r_{to} are the external radii of cement and tubing, respectively; T_{fi} and T_{fo} are the temperature of cold fluid injected in and hot fluid extracted out, respectively; U_{is} (or U_{oi}) is the coefficient of heat transfer between fluid flowing downward and the formation (or the fluid flowing upward), which can be evaluated via the following formula [81],

$$U_{si} = \left[\frac{r_w}{r_{ci}h_{conv,fi}} + \frac{r_w \ln(r_{co}/r_{ci})}{\lambda_{cas}} + \frac{r_w \ln(r_w/r_{co})}{\lambda_{cem}}\right]^{-1} \tag{12}$$

where r_{ti} is the internal radius of inner tubing; δ_i and δ_o are the thickness of inner and outer tubing wall, respectively; λ_{cas}, λ_{cem}, λ_{tub}, and λ_{ins} are the thermal conductivities of casing, cement, tubing and insulation, respectively; $h_{conv,f}$ is the convective heat transfer coefficient of fluid injected in ($h_{conv,\,fi}$) or extracted out ($h_{conv,\,fo}$), which can be evaluated as follows,

$$h_{conv,\,f} = \frac{\lambda_f Nu}{d_{hydraulic}} \tag{14}$$

$$U_{oi} = \left[\frac{r_{to}}{r_{ti}h_{conv,\,fo}} + \frac{r_{to}\ln(r_{ti}+\delta_i/r_{ti})}{\lambda_{tub}} + \frac{r_{to}\ln(r_{to}-\delta_o/r_{ti}+\delta_i)}{\lambda_{ins}} + \frac{r_{to}\ln(r_{to}/r_{to}-\delta_o)}{\lambda_{tub}} + \frac{1}{h_{conv,\,fi}}\right]^{-1} \tag{13}$$

where Nu is the Nusselt number, λ_f is fluid thermal conductivity.

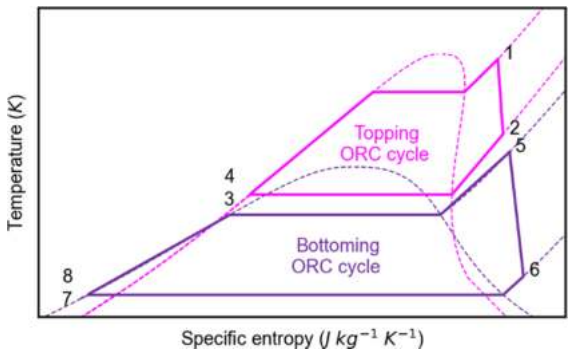

Fig. 5. A representative T-s diagram illustration of the two-stage cascaded ORC system. Numbers 1 to 8 represent the temperature and specific entropies of the corresponding points in Fig. 3.

2.2.6. Energy balance

The energy equation of cold fluid flowing downward in the annulus can be expressed as [56,55],

$$\left\{\frac{\partial\left[(\rho c_p)_{fi} A_i T_{fi}\right]}{\partial t} + \frac{\partial\left[(\rho c_p)_{fi} A_i v_{fi} T_{fi}\right]}{\partial x}\right\}dx = d\dot{Q}_{si} + d\dot{Q}_{oi} \tag{15}$$

where $(\rho c_p)_{fi}$ is the volumetric heat capacity of cold fluid injected; $A_i = \pi(r_{ci}^2 - r_{to}^2)$ is the area of annulus for liquid in; the heat flux from hot liquid $d\dot{Q}_{oi}$ can be expressed as,

$$\left\{\frac{\partial\left[(\rho c_p)_{fo} A_o T_{fo}\right]}{\partial t} + \frac{\partial\left[(\rho c_p)_{fo} A_o v_{fo} T_{fo}\right]}{\partial x}\right\}dx = -d\dot{Q}_{oi} \tag{16}$$

where $(\rho c_p)_{fo}$ and T_{fo} are the volumetric heat capacity and temperature of hot fluid extracted out, respectively; $A_o = \pi r_{ti}^2$ is the area of inner tubing for liquid out. The heat from the hot liquid flowing out can be ignored when the thermal performance of tubing insulation is good enough.

2.2.7. Hot thermal energy storage (HTES)

For the HTES between the AEW and the topping ORC cycle, the low-cost and mature dual-tank water storage system is selected (as depicted in Fig. 3), and water is used as both the TES material and HTF. The dual-tank design can supply hot energy to the ORC at a constant temperature, which is crucial to the operation of a power generating system. It also enables flexible and on-demand thermal energy supply to the district heating system of the local community and the ORC system by moderating the water flow rate. In this study, the water storage tanks are assumed to be well insulated, and the district heating supply temperature and hot water storage tank are the same. Therefore, considering a pinch point of 10 °C, the hot water storage temperature, and the topping ORC cycle evaporation temperature T_1 are 10 °C and 20 °C lower than the geothermal outlet temperature, respectively.

2.3. Two-stage cascaded ORC system

In this study, a two-stage ORC system (as shown in Fig. 3 and Fig. 5) design is adopted. In conventional geothermal power plants using

Table 3
Properties of the working fluids used in the ORC [9,2].

Cycle	Topping	Bottoming
Refrigerant	R1270 (Propylene)	R170 (Ethane)
Chemical formula	CH_2CHCH_3	CH_3CH_3
Critical point (°C)	91.06	32.17
Normal boiling point (°C)	−47.62	−88.58
Freezing point (°C)	−59	−183
Ozone Depletion Potential (ODP)	0	0
Global Warming Potential (GWP, 100-Years)	2	20

Table 4
ORC turbine and pump efficiency values used in this study.

Parameters	Values
Design point turbine isentropic efficiency, $\eta_{DP,\,turbine}$	60%
Turbine electromechanical efficiency, $\eta_{turbine,\,me}$	92%
Design point pump isentropic efficiency, $\eta_{DP,\,pump}$	70%
Pump motor efficiency, $\eta_{pump,mo}$	75%

single-stage ORCs, the temperature difference between the geothermal heat source and the cold source (usually ambient temperature) is around 100 °C. However, in this study, the temperature difference between the geothermal heat source and the LNG cold energy available (below −100 °C) source can be more than 200 °C. The temperature gap is so significant that no single working fluid can cover the whole range. Therefore, a topping cycle and a bottoming cycle are arranged in a cascaded manner to allow one working fluid to evaporate at around 100 °C and another to condense at around −100 °C. As pointed out by Mosaffa et al. [54], this configuration has a higher net power output compared to other ORC designs.

A thermodynamic model of the ORCs and an optimization model are developed in *Python*. The working fluids' thermophysical properties are taken from *CoolProp* [9]. Details of the ORC model, the working fluid selection, the development of the optimizer, and the off-design performance evaluation, are discussed in the following subsections.

2.3.1. Thermodynamic model

A steady-state first law of thermodynamics model was established for the ORC simulation. For simplicity, the heat exchangers and pipes' leakage, heat losses, and pressure drop are neglected. The pinch point temperature differences of the heat exchangers are fixed at 10 °C. Only gaseous and liquid phases are allowed in the turbines and pumps, respectively.

The equation of energy balance is applied to each component as:

Turbines:

$$\dot{W}_{turbine} = \dot{m}(h_{inlet} - h_{outlet})\eta_{turbine}\eta_{turbine,\,me} \tag{17}$$

where $\dot{W}_{turbine}$ (W) is the power production of the turbine, $\dot{m}$ (kg s^{-1}) is the mass flow rate of the working fluid, h (J kg^{-1}) is the specific enthalpy of the inlet and outlet fluid, $\eta_{turbine}$ is the isentropic efficiency of the turbine defined as,

$$\eta_{turbine} = \frac{h_{inlet} - h_{outlet}}{h_{inlet} - h'_{outlet}} \tag{18}$$

where h'_{outlet} is the enthalpy of the outlet working fluid if the entropy equals the inlet as $s_{inlet} = s'_{outlet}$, and $\eta_{turbine,\,me}$ is the electromechanical efficiency of the turbine.

Pumps:

$$\dot{W}_{pump} = \frac{\dot{m}(h_{outlet} - h_{inlet})}{\eta_{pump}\eta_{pump,\,mo}} \tag{19}$$

where $\dot{W}_{pump}$ (W) is the power consumption of the turbine, η_{pump} is the isentropic efficiency of the pump defined as,

$$\eta_{pump} = \frac{h'_{outlet} - h_{inlet}}{h_{outlet} - h_{inlet}} \tag{20}$$

where h'_{outlet} is the enthalpy of the outlet working fluid if the entropy equals the inlet as $s_{inlet} = s'_{outlet}$, and $\eta_{pump,\,mo}$ is the pump motor efficiency.

Heat exchangers:

$$\dot{Q} = \dot{m}_{hot}\left(h_{hot,\,inlet} - h_{hot,outlet}\right) = -\dot{m}_{cold}\left(h_{cold,inlet} - h_{cold,outlet}\right) \tag{21}$$

where $\dot{Q}$ (W) is the heat flow exchanged in the heat exchanger.

The overall efficiency of the two-stage ORC system is then defined as,

$$\eta_{ORC} = \frac{\dot{W}_{turbine,\,T} + \dot{W}_{turbine,\,B} - \dot{W}_{pump,T} - \dot{W}_{pump,B}}{\dot{Q}_{input}} \tag{22}$$

where T and B denote the topping and bottoming ORC cycle, respectively, $\dot{Q}_{input} = \dot{m}_T(h_1 - h_4)$ is the heat input from the AEW and the HTES to the topping cycle. In this study, the cold energy input from the LNG and CTES to the bottoming cycle is not included in the overall efficiency calculation since it is regarded as a "free" by-product of the LNG regasification process, which dissipates in the ambient air or seawater if not utilized.

To make sure the results from the *Python* ORC model are reliable, we have also developed a warning system that works in the same way as the commercial software *Aspen Plus*: any ORC working fluids or parameter sets that can lead to gaseous phase in the pumps, liquid phase in the turbines, and temperature cross in the heat exchangers, will be discarded. During the validation test of the ORC model, any parameter sets that can lead to warnings in *Aspen Plus* will also trigger the warning system of the *Python* model of this study. For parameter sets that will not trigger the warning system, the efficiency, temperature, pressure, and other outputs were found to be almost the same as the *Aspen Plus* simulations with only slight differences, probably due to the different material database. Therefore, the *Python* model was proved to have the same functionality as the *Aspen Plus* in terms of the first law of thermodynamic simulation of ORCs.

2.3.2. Working fluid selection

Various potential working fluids have been considered for the topping and bottoming cycle of the ORC system. A series of refrigerants are pre-selected from a comprehensive list of 79 commonly used commercial refrigerants [10] during the pre-selecting process according to the operating temperature ranges. In this study, only low global warming potential (GWP) and 0 ozone depletion potential (ODP) refrigerants were considered to reduce the AEW-ORC system's potential environmental impact. For the topping cycle, the pre-selected working fluids with the appropriate temperature ranges are R600a, R152a, R1234ze(E), R290, and R1270. For the bottoming cycle, only R1150 and R170 are available in the desired temperature range.

However, the geothermal fluid outlet temperature of AEWs can vary along with a wide temperature range from 60 to 120 °C. Due to the stringent requirements of the ORC model, only one working fluid pair, R1270 for the topping and R170 for the bottoming cycle, was found that has not triggered the warning system of the ORC model over the wide temperature range. Moreover, in a cascaded ORC system developed by Tian et al. [76], R1270 and R170 were found to have the lowest costs when used as the medium and low-temperature working fluids for similar temperature ranges of our ORC system. Therefore, R1270 and R170 are selected as the working fluid pair for this study. The parameters of the two low-environmental impact natural refrigerants selected are listed in Table 3.

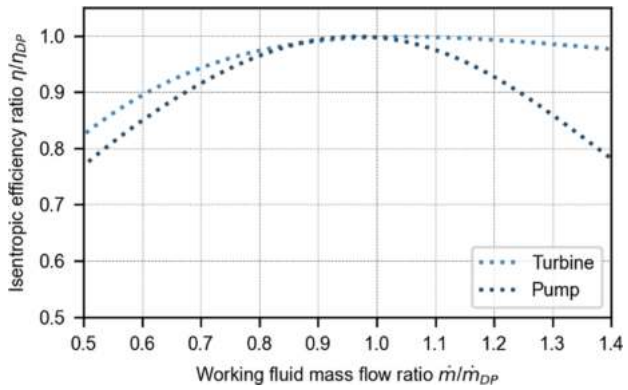

Fig. 6. Performance curves of the pumps and turbines.

Table 5
Composition of the LNG used in this study.

Component	Mole fraction
Methane	96.5222%
Nitrogen	0.2595%
Carbon dioxide	0.5956%
Ethane	1.8186%
Propane	0.4596%
i-Butane	0.0977%
n-Butane	0.1007%
i-Pentane	0.0473%
n-Pentane	0.0324%
n-Hexane	0.0664%

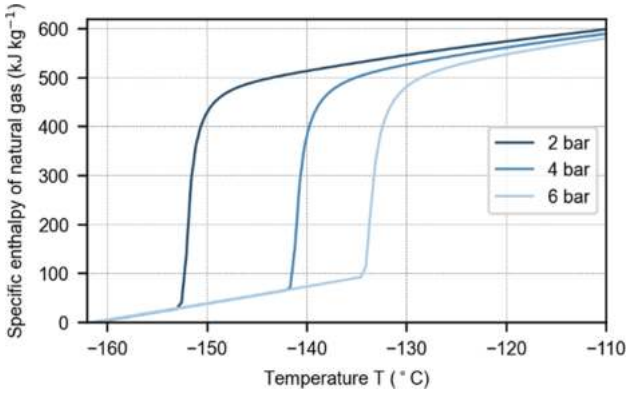

Fig. 7. Enthalpies of natural gas at various operating pressures.

2.3.3. Design point operation and design optimization

For the design point, fixed isentropic efficiencies ($\eta_{DP,turbine}$ and $\eta_{DP,pump}$) are used for the turbines and pumps. A wide range of efficiency values can be found in the literature: the overall turbine efficiency measured in different experimental studies ranges from 40% to 80% [44,12]), and the overall pump efficiencies used by various research ranges from 50% to 80% [6,71]. In this study, the efficiency values from Chen et al. [15] are adopted for the ORC model (as listed in Table 4).

For different applications, the designing goal of an ORC system can be either maximizing the power output or the efficiency [61,60]. In this study, maximizing the power output may lead to a dramatic decrease in the AEW formation temperature and the available geothermal energy of the AEW after years of operation. On the other hand, maximizing the efficiency of an AEW-ORC system at a stable geothermal fluid outlet temperature is equivalent to maximizing lifelong power production. Therefore, the overall efficiency of the whole ORC system, η_{ORC}, is selected as the objective function for the optimization of the ORC system.

To design a two-stage cascaded ORC system with the highest overall efficiency, Bayesian optimization using Gaussian Process [67], a fast and accurate optimization algorithm for black-box problems [85], is used as the algorithm to search for the best performing evaporating pressures, turbine pressure ratios, and mass flow rates for the topping and bottoming ORC cycles.

2.3.4. Off-design point operation

For the off-design point operation of the designed ORC system, the constant pressure control strategy with variable inlet guide vane is adopted in this study. Following the constant pressure operation, the evaporating pressure is fixed. As pointed out by Hu et al. [37,38], an ORC system under constant pressure operation has higher net work output in low mass flow rates compared to sliding pressure operation. The net work output is significantly lower than sliding pressure operation only in extremely high mass flow rates. Moreover, constant pressure operation can stabilize the temperature conditions regardless of the mass flow rates, which will significantly reduce the complexity in the control of a cascaded ORC system. The maximum heat and cold energy supply can be utilized without affecting the temperatures and pressures of the up and downstream systems of both the topping and bottoming cycles. Therefore, constant pressure operation is more suitable for our system than sliding pressure operation. In this study, we assume that, during the off-design operation, both the temperature and pressure conditions are maintained the same as the design point, while the mass flow rates of the working fluids are manipulated to match the variation in the LNG waste cold and geothermal energy supply.

For the heat exchangers in the cascaded ORC system, according to Hu et al. [37,38], during constant pressure operation, the enthalpy change is almost constant regardless of the working fluid mass flow rate, indicating that the outlet temperature of the working fluids does not change with the mass flow rate. A similar result was also found by Chatzopoulou et al. [14], who discovered the change in the effectiveness in the heat exchangers of an ORC system operating under constant pressure operation remains constant or varies in a small range subjected to dramatic heat source temperatures and heat source mass flow rates variations. Moreover, if the modular design can be adopted for the heat exchangers like the CTES system, fixed temperature and pressure control of the heat transfer can be further ensured. Therefore, in this study, the variation of the outlet temperatures of the heat exchangers is neglected for simplicity during off-design operation.

The isentropic efficiencies of the turbines and pumps, on the other hand, drop significantly during off-design operation. Therefore, in this study, the turbine isentropic efficiency is calculated using the performance curve available in Akar et al. [4] provided by a reliable manufacturer in the design of an ORC system for geothermal applications, and the pump efficiency is obtained from the performance curve used by Hu et al. [37,38] based on a multistage centrifugal pump in a real power plant. The fitted relationship between the isentropic efficiency ratio (isentropic efficiency during the off-design operation over the design point η/η_{DP}) and the working fluid mass flow rate ratio ($\dot{m}/\dot{m}_{DP}$) are plotted in Fig. 6. Moreover, since the $\dot{m}/\dot{m}_{DP}$ of the turbine efficiency curve provided by the manufacturer to Akar et al. [4] ranged from 50% to 140%, this study will also use this range as the working fluid mass flow rate range of the ORC system: for the sake of durable operation of the facilities, we assume that the ORC will be bypassed if $\dot{m}/\dot{m}_{DP}<50$ %, and only 140% of the $\dot{m}_{DP}$ will be used in the ORC if $\dot{m}/\dot{m}_{DP}>140\%$.

2.4. LNG cold extraction and storage in CTES

The high grade (low temperature) part of the LNG cold energy is supplied to the CTES, and the low grade (high temperature) part can be delivered to the other cold demand. Due to the lack of suitable liquid sensible storage materials at cryogenic temperatures and the low volumetric energy density of solid sensible storage materials [86], phase

Table 6
Properties of the PCM used in the CTES.

Properties	Values
Phase change temperature	−114 (°C)
Thermal conductivity	0.20 (W m^{-1} K^{-1})
Density	789.3 (kg m^{-3})
Volumetric specific heat capacity	1.499 (MJ m^{-3} K^{-1})
Volumetric latent heat	67.88 (MJ m^{-3})
Estimated cost for mass production	2 (USD_{2020} kg^{-1})

Table 7
Properties of the HTF (3M™ Novec™ 7000) used in the intermediate heat transfer loop [1].

Properties	Values
Pour point	−122 (°C)
Thermal conductivity	0.075 (W m^{-1} K^{-1})
Density	1400 (kg m^{-3})
Volumetric specific heat capacity	1300 (MJ m^{-3} K^{-1})
Kinematic viscosity (at −114 °C)	10 (cSt)

change material (PCM) is selected for the CTES between the LNG satellite station and the bottoming ORC cycle. A PCM-based CTES system has high energy density and supplies cold energy at a constant temperature, similar to the dual-tank HTES system.

2.4.1. PCM selection

The phase change temperature of the PCM should be compatible with the evaporation temperature of the LNG. In this study, the composition of the gulf gas mixture (NIST1) [48,41] (as listed in Table 5) taken from *CoolProp* [9] is used to calculate the thermophysical properties of the LNG, and the lower heating value is calculated as 48.85 MJ kg^{-1} [78].

The typical operating pressure of the LNG storage tank of a satellite station is 4 to 6 bar, and the gas network is between 2 and 4 bar [22]. Therefore, in this study, the pressure of LNG is selected as 4 bar, which is a typical nominal discharging pressure of satellite LNG stations [22,84]. At this pressure, most of the latent heat of vaporization is released between −143 and −135 °C (as depicted in Fig. 7). Moreover, during the operation of the LNG terminal, the discharge temperature can deviate from the design point. For example, in an LNG cold energy air separation system [35], although the designed LNG discharge temperature is −147 °C, the real discharge temperature varies between −146 and −126 °C. Therefore, in this study, the PCM should have a phase change temperature of around −120 to −110 °C to make more use of the cold energy and exergy released during the phase change.

Limited commercial PCM products are available in this temperature range [86]. In this study, the PCM developed at the Thermal Energy Systems Lab @ Nanyang Technological University [75] with a phase change temperature of −114 °C is selected. The properties of the PCM are listed in Table 6.

2.4.2. CTES design and optimization

Shell-and-tube is chosen as the storage type for this study due to its maturity in design and high volumetric energy density. An ε-NTU method is used to design the CTES unit. The method was proposed by Tay et al. [74] and further validated by us in a previous study [88]. In the intermediate heat transfer loop, 3M™ Novec™ 7000 [1] is selected as the HTF to transfer cold energy from the LNG to the CTES and the ORC. The properties of the HTF are listed in Table 7.

A modularized design is adopted in this study for the CTES, in which more than one CTES module can be charged or discharged in parallel when the LNG cold energy supply changes. Since the capital cost of a TES unit is mainly determined by its heat transfer area [88], the total cost of a modularized CTES system will not be significantly higher than a single CTES unit as long as the modules are well designed to reduce the dead volumes.

During the designing of the CTES modules, since the cold energy and power demands are fixed, the design should focus on minimizing both the investment cost and the operational cost while meeting the desired charging and discharging power requirements. Therefore, in this study, the depreciated payback period (PBP) [64] is selected to be the objective function, which involves both the investment cost (CAPEX) and the operational cost (OPEX).

$$PBP = \frac{-\ln\left(1 - r\frac{CAPEX}{Profit}\right)}{\ln(1+r)} \tag{23}$$

where r is the discount rate, $CAPEX$ is the investment cost of the CTES, and $Profit$ is the annual cash flow, mainly affected by the pumping cost of the CTES. Therefore, by using the PBP as the objective function, the optimization will reduce the CAPEX and the OPEX of the CTES at the same time. The Non-dominated Sorting Genetic Algorithm II (NSGA-II) [11], a widely used multi-objective genetic algorithm, is used to optimize the design of the CTES modules.

2.5. Economic models

In a conventional geothermal power plant, the CAPEX can be divided into three parts: the drilling cost, C_{Drilling}, the power plant cost, $C_{\text{Power plant}}$, and the other costs, C_{Other}, where C_{Other} includes the geothermal fluids transportation system, the communication system, the management costs, the miscellaneous costs, and so on.

$$C_{\text{Geothermal}} = C_{\text{Drilling}} + C_{\text{Power plant}} + C_{\text{Other}} \tag{24}$$

In this study, since AEW is used, C_{Drilling} can be saved. $C_{\text{Power plant}}$ will be the investment cost of the ORC system, C_{ORC}. The AEW renovation costs will be formed only by the other costs of a conventional geothermal plant. The cost related to the satellite LNG station is also neglected since the stations are already built or planned to be built to meet the natural gas demand with the cold energy wasted if not used for power generation. Therefore, by including the cost for the CTES, the CAPEX structure of the system is:

$$C_{\text{Geothermal}} = C_{\text{AEW Renovation}} + C_{\text{ORC}} + C_{\text{CTES}} \tag{25}$$

where $C_{\text{AEW Renovation}}$ can be assumed to equal the C_{Other} of a conventional geothermal power plant of the same scale.

2.5.1. AEW renovation cost

According to the investment cost breakdown data of a commercial geothermal project collected by the World Bank, the other costs take 31% of the total investment cost [30], a share similar to the estimation of Kurnia et al. [46]. However, a detailed estimation of $C_{\text{AEW Renovation}}$ item by item can be considerably complex. Therefore, in this study, a simple method is adopted by assuming the $C_{\text{AEW Renovation}}$ to be equal to 31% of a conventional geothermal project of the same scale. According to the International Renewable Energy Agency (IRENA) [39], the costs for small-scale and low-temperature resource binary plants (including ORC) range from 5,000 to 10,000 USD per kW_{ele}, higher than those with better geothermal reservoirs and resources. The average specific investment cost (SIC) for small geothermal projects (less than 1 MW_{ele}) in the latest IRENA renewable power generation costs report, 9509 USD_{2020} per kW_{ele} [40], is hence used as the $SIC_{\text{Geo, equivalent}}$ in this study since the temperature range of our system is low and the scale is small.

Therefore, $C_{\text{AEW Renovation}}$ can be estimated as:

$$C_{\text{AEW Renovation}} = \alpha_{\text{other}} SIC_{\text{Geo, equivalent}} P \frac{\eta_{\text{world average}}}{\eta} \tag{26}$$

where $\alpha_{\text{other}} = 31\%$ is the share of the other costs in a conventional geothermal plant, $\eta_{\text{world average}}$ is the worldwide average efficiency of

Table 8
Assumptions and values taken for the economic models.

Parameter	Value	Reference
Discount rate,r	5%	[28]
World average geothermal power efficiency, $\eta_{\text{world average}}$	12%	[40]
CEPCI of 2020,$CEPCI_{2020}$	596.2	[51]
Operational costs,$OPEX$	2% of CAPEX	[30]
Lifetime of the system,n	25 (years)	[40]
Specific investment cost of utility-scale battery,SIC_{battery}	322 (USD_{2020} kWh_{ele}^{-1})	[23]

Table 9
Input parameters of the thermal model for solving recovered fluid temperature.

Parameter	Symbol	Value	Unit
Inner radius of inside tubing	r_{ti}	0.031	m
Inner radius of outside tubing	r_{to}	0.0572	m
Inner radius of casing	r_{ci}	0.0807	m
Outer radius of casing	r_{co}	0.0889	m
Thickness of cement	δ_{cem}	0.0347	m
Thickness of inside tubing	δ_{i}	0.0055	m
Thickness of outside tubing	δ_{o}	0.0063	m
Thickness of insulation	δ_{ins}	0.0144	m
Thermal conductivity of tubing	λ_{tub}	57	$W\,m^{-1}\,K^{-1}$
Thermal conductivity of insulation material	λ_{ins}	0.027	$W\,m^{-1}\,K^{-1}$
Thermal conductivity of casing	λ_{cas}	57	$W\,m^{-1}\,K^{-1}$
Thermal conductivity of the cement	λ_{cem}	0.46, 2.3	$W\,m^{-1}\,K^{-1}$
Thermal conductivity of the formation	λ_{s}	1.8	$W\,m^{-1}\,K^{-1}$
Volumetric heat capacity of casing	$(\rho c_{\text{p}})_{\text{cas}}$	4.68e6	$J\,m^{-3}\,K^{-1}$
Volumetric heat capacity of cementation	$(\rho c_{\text{p}})_{\text{cem}}$	3e6	$J\,m^{-3}\,K^{-1}$
Injection pressure	P_0	0.3–0.9	MPa
Entrance temperature of inlet working fluid	$T_{\text{fi}}(x=0)$	25	℃
Formation temperature at the earth surface	T_0	15	℃
Velocity of inlet working fluid	v_{f}	0.1–0.3	$M\,s^{-1}$
Formation temperature gradient	∇T	0.03–0.06	$K\,m^{-1}$
Length of well in the vertical direction	L_{v}	3, 4, 5, 6	km
Length of well in the horizontal direction	L_{h}	0, 0.5, 1	km

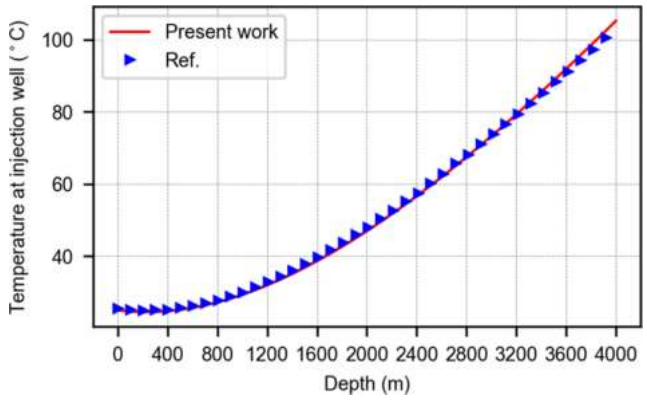

Fig. 8. Variation of inlet fluid temperature T_{fi} along well depth in comparison with results from [20,21]: simulation results are plotted after 300 days of operation; working fluid is R143a; formation temperature gradient is 0.033 $K\,m^{-1.}$

geothermal plants, and η is the overall efficiency of the AEW geothermal plant.

Table 10
ORC model validation results.

Parameters	Experiment [89]	Model (this study)	Error
ORC system efficiency (average)	4.46%	4.47%	0.2%
Turbine outlet temperature (average)	51.1 °C	51.8 °C	0.7 °C

2.5.2. ORC cost

To estimate the C_{ORC}, various market surveys of commercially deployed ORC projects and component-to-component-based cost models are available in the literature. For example, Strzalka et al. [73], van Kleef et al. [79], and Pantaleo et al. [58] have summarized the costs of various recent market surveys and estimation methods. However, the difference between model estimates and market survey data is not insignificant for ORC modules with power outputs ranging from 20 to 100 kW_{ele}, which is the scale of interest in this work. As pointed out by van Kleef et al. [79], around this power output range, the estimation models tend to either significantly overestimate or underestimate the specific investment cost, SIC_{ORC}. The SIC_{ORC} from different estimation methods ranges between 1400 USD_{2020} kW_{ele}^{-1} and 14,700 USD_{2020} kW_{ele}^{-1}, while the market values are within a much smaller range between 2,400 USD_{2020} kW_{ele}^{-1} and 8,800 USD_{2020} kW_{ele}^{-1}. The results are plotted in Fig. A.1. Therefore, in this study, the SIC_{ORC} (in USD_{2020} kW_{ele}^{-1}) is obtained from the correlation generated from the market survey data summarized during the past 10 years (as shown in Fig. A.2):

$$SIC_{\text{ORC}} = -678ln(P_{\text{ORC}}) + 6725.4 \tag{27}$$

and the total C_{ORC} is the sum of the costs of the topping and bottoming cycles as $C_{\text{ORC}} = SIC_{\text{ORC,T}}P_{\text{T}} + SIC_{\text{ORC,B}}P_{\text{B}}$.

2.5.3. CTES cost

Since no market data is available for the CTES cost, C_{CTES}, the estimation method developed in a previous study by the authors [88] based on the Seider method [68] is adopted as:

$$C_{\text{CTES}} = C_{\text{PCM}} + C_{\text{HEX}} \tag{28}$$

C_{CTES} contains two parts, the PCM cost, C_{PCM}, and the HEX cost, C_{HEX}, by assuming the CAPEX of the containment of the CTES module is equal to a shell-and-tube heat exchanger of the same configuration, which is calculated as:

$$C_{\text{HEX}} = C_{\text{Base}}F_{\text{M}}F_{\text{L}}\frac{CEPCI_{2020}}{500} \tag{29}$$

For the base cost, $C_{\text{Base}} = exp\left\{11.0545 - 0.9228[\ln(10.7639A)] + 0.09861[\ln(10.7639A)]^2\right\}$ for chemical engineering plant cost index (CEPCI) of 500, and A is the heat transfer area. The material factor, $F_{\text{M}} = 1.3$ is selected for aluminum alloy [69]. Since both the HTF and PCM are non-corrosive, aluminum alloy, which is a commonly used material for LNG evaporators, is selected to build the CTES modules due to its good performance for cryogenic applications [87]. The length factor, F_{L}, is taken from Seider et al. [68] for various tube lengths.

The other assumptions and values used in the economic models are listed in Table 8.

3. Results and discussion

3.1. Model validation

3.1.1. AEW model validation

Parameters involved in the AEW model development are listed in Table 9. As for the system for thermal energy exploitation, the temperature of the working fluid T_{fo} or T_{fi} is of interest. To validate the

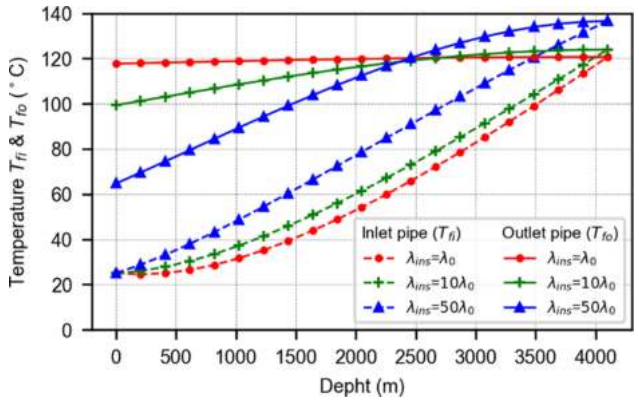

Fig. 9. Temperature distribution of fluid flowing downward and upward in the inlet (T_{fi}) and outlet (T_{fo}) pipe channels under the impact from insulation properties of the inner pipe λ_{ins}: simulation results are plotted after 300 days of operation; the working fluid is water; λ_0 is 0.0027 W m^{-1} K^{-1}; The well depth is 4000 m starting from 0 m on the surface; the temperature gradient is 0.04 K m^{-1}.

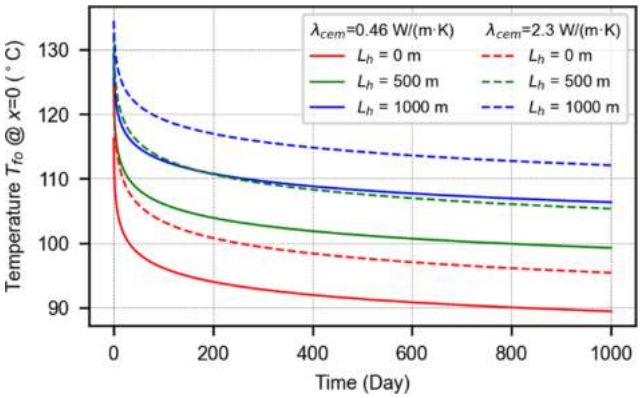

Fig. 10. Recovered water temperature $T_{fo}|_{x=0}$ (the value of T_{fo} at 0 m well depth in Fig. 9) under impact from different lengths of the horizontal extension L_h and thermal conductivities of the cement layer λ_{cem}: simulation results are plotted within 1000 days of operation; well vertical length is 4000 m; temperature gradient is 0.04 K m^{-1}.

feasibility of the current model, one case study with a depth varying T_{fi} is illustrated in Fig. 8, which is compared with the results of another work [20,21], where R143a is taken as the working fluid, and the formation temperature gradient is 0.033 K m^{-1}. Meanwhile, the inner pipe for transporting hot fluid is of perfect insulation; thus, the temperature of recovered fluid $T_{fo}|_{0\le x\le L}$ equals $T_{fi}|_{x=L}$, which is a horizontal line and thus not shown in Fig. 8. The results from our model almost overlaped with the reference data.

3.1.2. ORC model validation

Using the same equations and assumptions as described in Section 2, a single-stage version of the ORC model is validated against the experimental results of Yang et al. [89]. The same working fluid and working conditions of the experiment were applied to the model. By using the efficiency values of Chen et al. [15] (as listed in Table 4), which is from the same group of researchers who conducted the experimental study [89], the average error of the ORC efficiency is 0.2%, and the average difference of turbine outlet temperature is 0.7 °C (Table 10). Therefore, though higher turbine and pump efficiencies are also reported in other literature, this research is based on these experimentally validated results.

3.2. Application of the geothermal model to the AEW design

There would be heat transfer between the hot and cold fluid when the inner pipe for transporting hot fluid is not perfectly insulated, which can affect the fluid temperature in both inlet and outlet pipes. Considering the insulation layer of three significantly different thermal conductivities, we can clearly see the differences in the various patterns of inlet and outlet fluid temperatures, as demonstrated in Fig. 9. Under good thermal insulation $\lambda_{ins} = \lambda_0$, the temperature of inlet fluid (dashed line) within the starting 500 m would decrease first and then increase, as the entrance temperature of the water is higher than the formation temperature at the earth's surface, thus causing heat transfer from downward liquid to the surrounding formation. Nevertheless, after weakening the insulation capability by 10 or 50 times with λ_{ins} equal to $10\lambda_0$ or $50\lambda_0$, we no longer see this transition process with the temperature dropping due to extra heat supply from the hot fluid. Though increase of λ_{ins} can derive higher temperature of inlet fluid along well depth (dashed line), the temperature of outlet fluid (solid line) is declining with a higher rate of decrease, and the recovered temperature of the water $T_{fo}(x = 0)$ is dropping sharply. Therefore, special attention should be paid to the insulation capability of the outlet pipe. Otherwise, the overall system thermal performance would be significantly affected.

Considering that there are many AEWs with horizontal extension and the possible degradation of cemented layer, the impacts of the length of the horizontal extension and thermal conductivity of cemented layer on the recovered fluid temperature are explored, as presented in Fig. 10, where water is selected in this study due to cost and environmental considerations.

Overall, the recovered fluid temperature drops with the operation time, especially within the initial 100 days, where there is a dramatic declining stage, as the extraction of thermal energy can reduce the temperature of rock formation adjacent to the wellbore structure, and thus lead to a smaller temperature difference between the external surface of the wellbore T_w and the inner fluid flowing downward T_{fi}. However, the rate of decrease would drop to a very small value after around 200 days of operation, and the existence of horizontal extension can bring about a substantial increase of the recovered temperature, with a 10℃ increase after adding the first 500 m, and an extra 5 ℃ increase after adding another 500 m. While improving the heat transfer capability of the cement layer would lead to a further increase in the recovered temperature.

Before building a geothermal system, a more urgent issue is associated with the system capacity after a long time of operation; therefore, more case studies were conducted to assess the recovered fluid temperature $T_{fo}|_{x=0}$ after 20 years' operation and the corresponding ORC overall system energy efficiency η_{ORC} with $T_{fo}|_{x=0}$, considering the possible temperature gradient, length of vertical well and horizontal extension, and injection velocity.

According to Gadd et al. [29], a third-generation district heating system requires a supply temperature of above 80 °C. In some first and second-generation district heating systems, the supply temperature of required is even higher than 110 °C. Hence, the geothermal outlet temperature should be above 90 °C to be used for district heating. The intermediate heat transfer loop inlet temperature is selected to be −120.0 °C, which is the lowest operating temperature of 3M^{TM} Novec^{TM} 7000 according to the manufacturer's recommended range [1]. According to results presented in Fig. 11, obvious patterns can be found: a) a higher temperature gradient ∇T can derive a higher recovered temperature $T_{fo}|_{x=0}$ and overall ORC system efficiency η_{ORC}; b) for the cases when $T_{fo}|_{x=0}$ is greater than 90°C, the overall ORC system efficiency η_{ORC} ranges between 23.2% and 25.3%, while there are no data points under $\nabla T = 0.02$ K m^{-1}, and only four under $\nabla T = 0.03$ K m^{-1}. The results demonstrate that with the LNG cold, the ORC efficiency can be significantly higher than the other research that utilizes the geothermal energy in AEWs, which are generally below 10% due to the low $T_{fo}|_{x=0}$

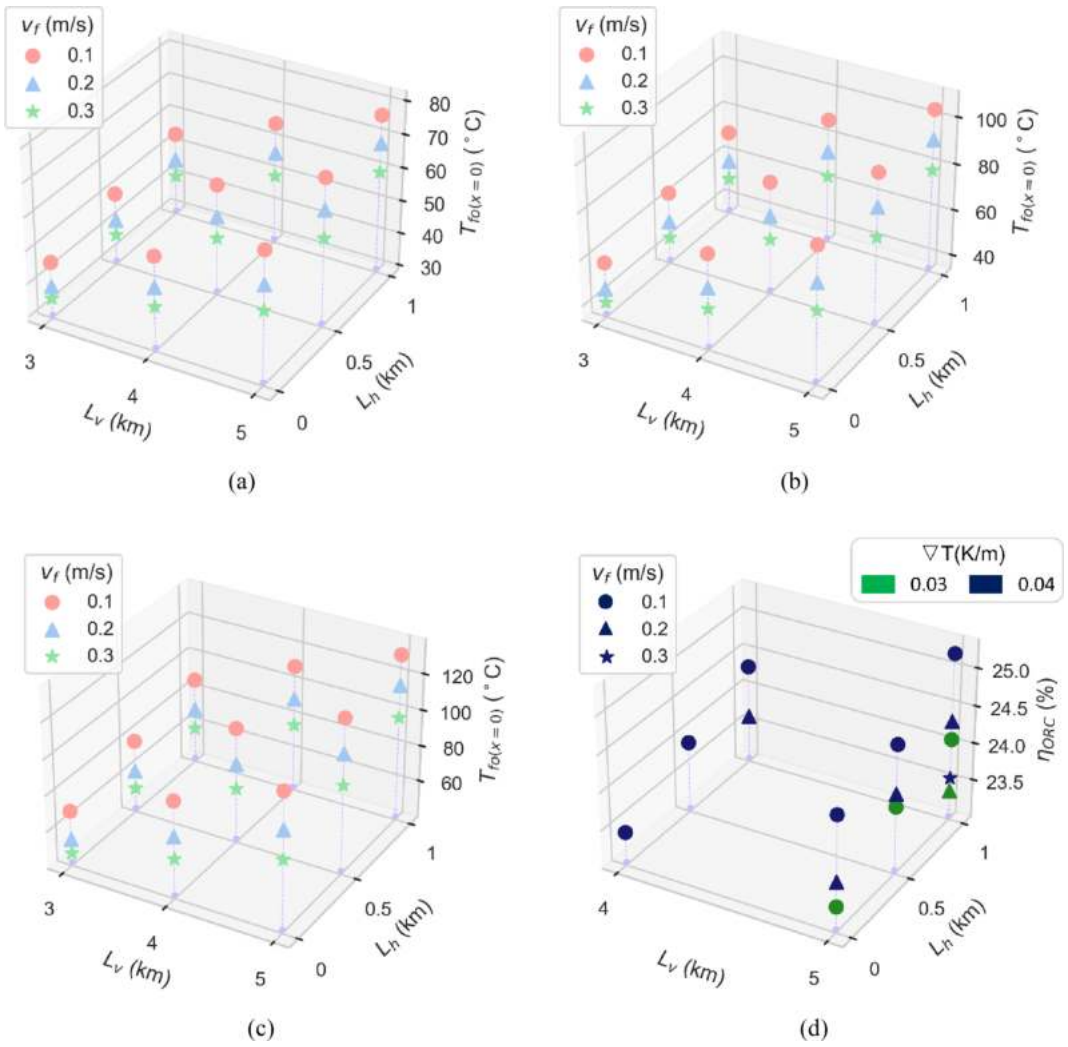

Fig. 11. Recovered water temperature with temperature gradient ∇T equal to (a) 0.02 K m^{-1}, (b) 0.03 K m^{-1}, and (c) 0.04 K m^{-1}, and (d) system overall energy efficiency η_{ORC} when $T_{fo}|_{x=0} > 80$ °C, considering varying well vertical length L_v, horizontal extension length L_h, and injection velocity of working fluid v_f. Simulation results are plotted after 20 years of operation. Thermal conductivity of cement layer $\lambda_{cem} = 2.3$ W m^{-1} K^{-1}).

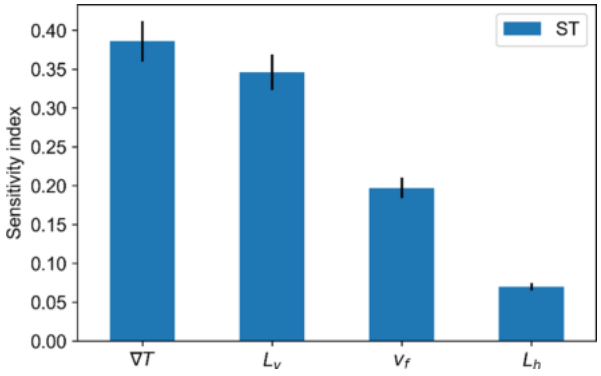

Fig. 12. Sensitivity analysis of impact factors for the recovered temperature from AEW based geothermal system.

values. Moreover, both $T_{fo}|_{x=0}$ and η_{ORC} are declining with increasing injection velocity v_f, but ascending with increasing vertical length L_v and horizontal extension L_v. Therefore, AEW with a temperature gradient lower than 0.02 K m^{-1} are not recommended if district heating is required, especially when high injection velocity is in demand; AEWs with horizontal extension are strongly recommended.

Sensitivity analysis further validated the conclusions derived above, as presented in Fig. 12, the recovered fluid temperature $T_{fo}|_{x=0}$ is the most sensitive to the variation of temperature gradient ∇T and the vertical well length L_v, then comes the injection velocity of working fluid v_f. Though the value of sensitive index in the length of horizontal extension L_h is the smallest, it does not mean that L_h is not important to the improvement of the system's thermal performance but only reveals that the response of $T_{fo}|_{x=0}$ is less sensitive to L_h compared with the other parameters under the current parameter scope. In the other words, the sensitivity index of L_h can be remarkably different if its values are two or three times larger than the current ones. The relationship between $T_{fo}|_{x=0}$ and the four impact factors (∇T, v_f, L_v, and L_h) can be fitted into a linear equation with an R-square value of 0.9454: $T_{fo}|_{x=0} = 33.091\widetilde{\nabla T} - 23.641\widetilde{v_f} + 31.301\widetilde{L_v} + 14.083\widetilde{L_h} + 246.266$ (K), where $\widetilde{var} = (var - var_{min})/(var_{max} - var_{min})$, and var, var_{min}, var_{max} represent a variable (∇T, v_f, L_v, or L_h), and its minimum and maximum value, respectively. The absolute value of each coefficient denotes the degree of influence of each variable, while the associate plus or minus sign denotes positive or negative impact.

3.3. Application of the ORC model to the ORC performance analysis

To reveal the role of CTES in such a system, a case study using the

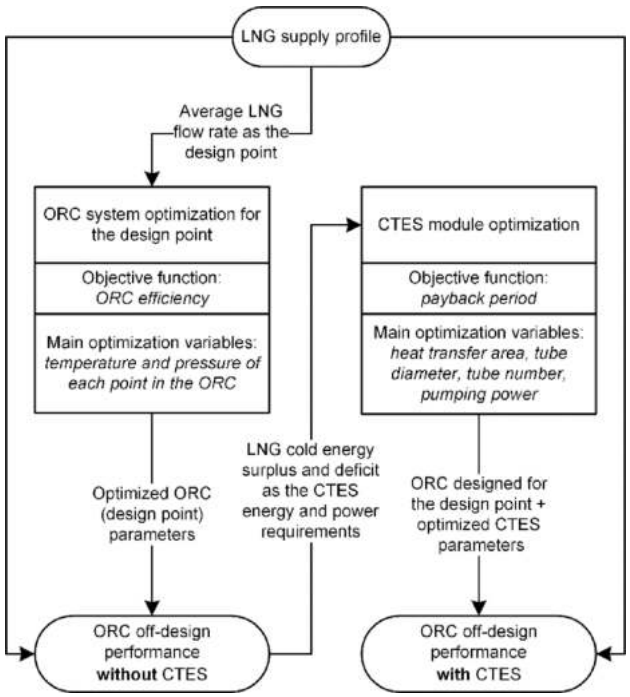

Fig. 13. Flow diagram of the ORC off-design performance comparison with and without CTES. The average LNG flow rate is used as the design point for the ORC optimization using efficiency as the objective function. The optimized ORC is subjected to the LNG supply profile to calculate the off-design performance without CTES. The LNG cold energy surplus and deficit are hence used to determine the requirements of the CTES modules, and the CTES modules are optimized using the payback period as the objective function. The ORC performance with the CTES is then generated.

real-world LNG demand profile in Fig. 2 is conducted to compare the ORC system performance with and without the CTES modules. Since no system of extracting geothermal energy from AEW for both district heating and power generation has been commercially deployed and put into long-term operation, there is a lack of typical operating data on the AEW geothermal energy supply and demand. Therefore, in this section, only the influence of the LNG demand fluctuation on the ORC system is considered, assuming the HTES supplies stable geothermal energy to the ORC system.

The process of the ORC system performance evaluation with and without CTES modules is illustrated in Fig. 13. The average LNG mass flow rate of Fig. 2 is taken as the design point to obtain the parameters of an optimized ORC system. In this case study, on the heat source side, the geothermal fluid outlet temperature is assumed to be 110 °C, which is a typical supply temperature for district heating; on the cold sink side, the HTF temperature of the intermediate heat transfer loop is fixed at −120.0 °C. The working fluids' mass flow rates, temperatures, and pressure levels are then optimized to seek optimal ORC efficiency. As a result, an optimized two-stage ORC system with an efficiency of 24.2%

Table 11
Parameters of the optimized CTES module designed.

Parameters	Values
Charging power (desired)	35.0 (kW_{cold})
Charging power (designed)	34.8 (kW_{cold})
Difference between the designed and desired charging power	1.55%
Maximum number of CTES modules needed during charging	6 (-)
Tube diameter	17.1 (mm)
Number of tubes	81 (-)
Total heat transfer area	1084.6 (m^2)
Pumping power (average)	1.05 (kW_{ele})
Average number of CTES modules needed during discharging	1.45 (-)

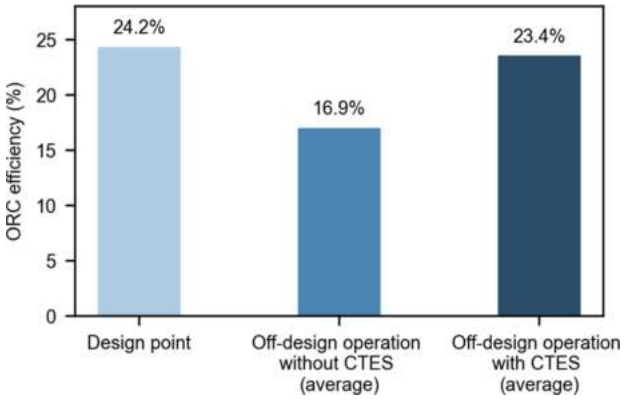

Fig. 15. ORC efficiency comparison between the design point and off-design operation with and without CTES.

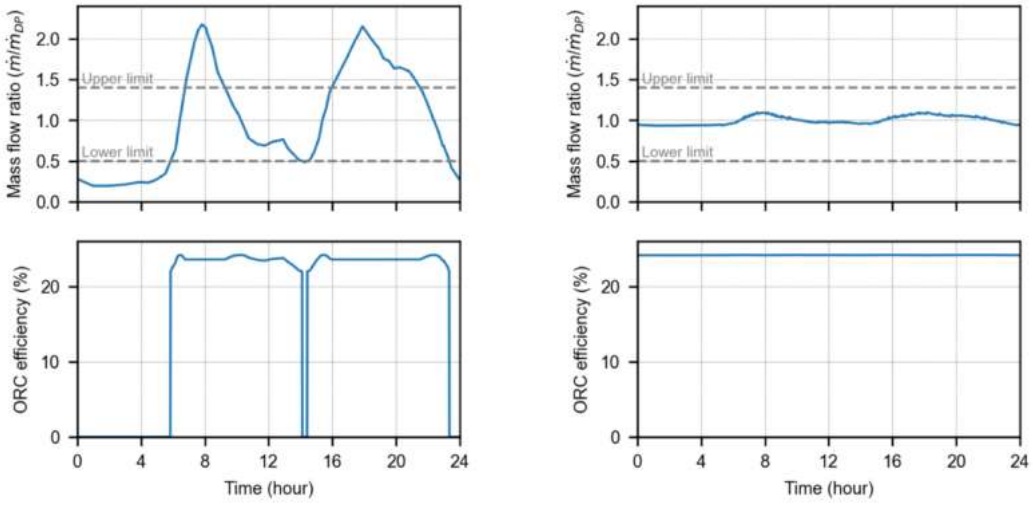

(a) Without CTES (b) With CTES

Fig. 14. Mass flow rate ratio and efficiency of the ORC system during off-design operation without (a) and with (b) CTES.

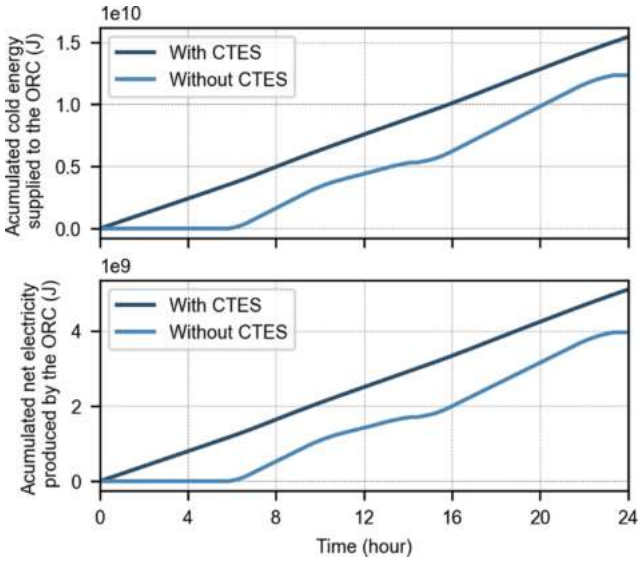

Fig. 16. Cold energy supplied to the ORC and ORC net electricity produced with and without CTES modules during off-design operation.

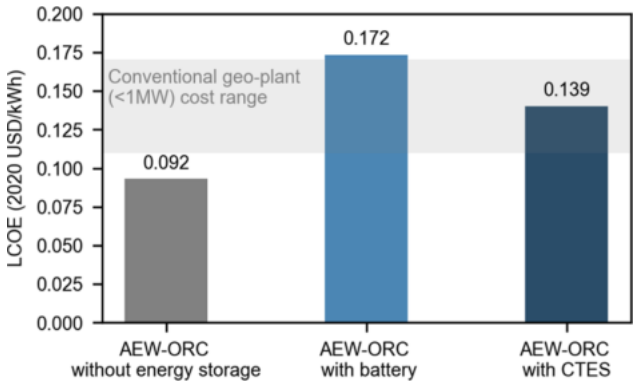

Fig. 17. LCOE comparison for the AEW-ORC system without cold energy supplied to the ORC and ORC net electricity produced with and without CTES modules during off-design operation.

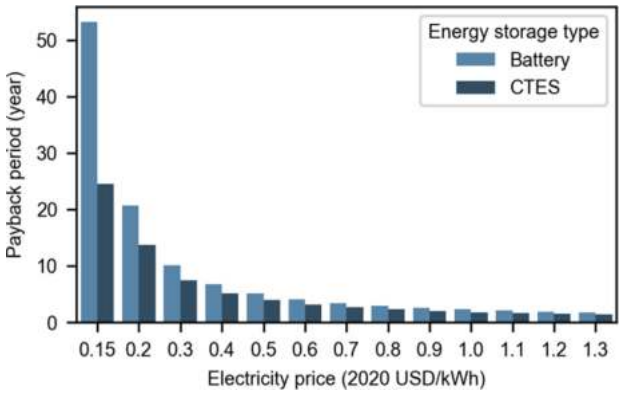

Fig. 18. PBP comparison for the AEW-ORC system with CTES and battery as the energy storage technology.

and net electrical power output of 59.1 kW_{ele} was obtained. The performance of this ORC system is then used as the baseline for comparison.

For the off-design operation performance without CTES, the optimized ORC system for the design point was subjected to the varying LNG supply profile in Fig. 2. The results are plotted in Fig. 14 and Fig. 16, and listed in Table 12. Under the constant pressure control strategy as described in Subsection 3.2, the ORC efficiency, cold energy supplied, and net electricity generated during the 24-hour operation are calculated. As shown in Fig. 14 and Fig. 16, when $\dot{m}/\dot{m}_{DP}$ is below the lower limit of 0.4, η_{ORC} and electricity generation are zero since the ORC system is bypassed; when $\dot{m}/\dot{m}_{DP}$ is higher than 1.4, η_{ORC} is fixed at a value lower than the design point ($\eta_{ORC} = 23.6\%$ when $\dot{m}/\dot{m}_{DP} = 1.4$), resulting in average efficiency of 16.9%, nearly one-third less than the design point, leading to the overall electricity production to be only 77.5% of the designed point.

For the off-design operation performance with CTES, the CTES modules are optimized. The CTES modules should be able to store all the surplus LNG cold energy during a day, and the charging and discharging power is enough to make use of all the surplus cold power and supply all the cold power deficit. The desired charging and discharging power of one CTES module is selected to be the lowest amount of LNG cold energy supply. In the optimization of the CTES module, the constraints are set as 1) the storage capacity, charging and discharging power are within 1% of the desired values, and 2) the pumping work is limited to be less than 3 kW_{ele}. As a result (as presented in Table 11), the design with the lowest PBP is selected as the optimized CTES module with the best compromise between the investment and operation cost. The difference between the designed and desired charging power is 1.55%, and the pumping power is around 1 kW_{ele}.

When subjected to the LNG cold energy supply in Fig. 2, by controlling the number of CTES modules working in parallel, the cold energy charging and discharging power can vary along with the LNG supply profile. The HTF flow is evenly distributed in the CTES modules at all times, ensuring the operation of each CTES module is close to the nominal charging conditions. During the charging phase, maximumly 6 CTES modules will be needed to work in parallel to capture the maximum amount of LNG cold energy supplied. During the discharging process, 1.45 modules on average are needed to deliver the stored cold energy to the ORC system, making the power output of the ORC almost the same as the design point operation. As shown in Fig. 14b, the mass flow ratio fluctuates only in a small range (less than 10% of the design point, compared to more than 100% for the ORC without CTES), making the efficiency kept at almost the same of the design point operation. As shown in Fig. 15, due to the pumping power of the CTES, the efficiency of the ORC system slightly dropped from 24.2% to 23.4%. However, it is 38.5% higher than the average η_{ORC} of 16.9% without the CTES modules.

Table 12
Summary of the ORC system performance with and without CTES during off-design operation compared with the design point.

Cases	ORC efficiency		LNG cold energy utilized		Net electricity generated	
	Values (%)	Ratio to the design point (%)	Values (10^9 J_{cold})	Ratio to the design point (%)	Values (10^9 J_{ele})	Ratio to the design point (%)
Design point	24.2%	–	15.43	–	5.11	–
Off-design operation without CTES	16.9% (average)	69.8%	12.34	80.0%	3.96	77.5%
Off-design operation with CTES	23.4% (average)	96.8%	15.40	99.8%	4.95	96.9%

Moreover, 99.8% of the available cold energy can be captured and supplied to the ORC system, enabling the ORC system to produce more electricity compared to the off-design operation without CTES. As presented in Fig. 16, combining the high ORC efficiency and high cold energy utilization rate, 4.95×10^9 J_{ele} of electricity can be generated. The net power output is 25.0% higher than the off-design operation without CTES. The overall performance of the design point, and off-design operation with and without CTES are summarized in Table 12.

Besides generating more power at a higher efficiency, the CTES modules ensure the stable operation of the ORC system at optimal conditions. The accumulated electricity production curve with the CTES in Fig. 16 is almost a straight line, indicating the power production is much more stable than the ORC operation without CTES, making it more friendly to the utility grid. Therefore, the CTES can play an essential role in the integrated AEW heat and LNG cold energy utilization system by significantly increasing the ORC efficiency and net electricity output when subjected to the highly fluctuated LNG demand profile. It also enables the AEW-ORC system as a possible source for peak load shifting or a virtual power plant, which will bring extra economic benefits by selling the electricity at a higher price.

3.4. Techno-economic analysis

The levelized cost of electricity (LCOE), is first analyzed for the AEW-ORC system,

$$LCOE = \frac{CAPEX + \Sigma_1^n \frac{OPEX}{(1+r)^t}}{\Sigma_1^n \frac{w_{net}}{(1+r)^t}} \quad (29)$$

where *CAPEX* is the investment cost of the whole system, *OPEX* is the annualized operational cost, w_{net} is the net electricity generation of the year t, and n is the system's lifetime taken from Table 8. The LCOE results for the AEW-ORC system with and without energy storage are illustrated in Fig. 17.

In general, the results match well with the range of LCOE values of conventional geothermal power plants below 1 MW_{ele}, which is around 0.11 to 0.17 USD_{2020} kWh_{ele}^{-1} [40]. The LCOE without energy storage, 0.092 USD_{2020} kWh_{ele}^{-1}, is less than the range of conventional geo-plants, indicating the utilization of AEW can significantly reduce the LCOE by saving the drilling costs, and more satellite LNG stations can be planned to be collocated with the AEWs to produce electricity. However, unlike a conventional geothermal plant whose power production is stable and controllable, the power production of this system without energy storage is as intermittent, unstable, and unpredictable as a renewable energy source like photovoltaic or wind. Such a power source can only be used for a large electricity grid equipped with enough power reserves to deal with the intermittency of the AEW power plant, or equipped with enough electricity storage capacities, such as li-ion batteries, to be used in a microgrid or supplied to the users nearby.

By including the CTES modules, the LCOE will increase to 0.139 USD_{2020} kWh_{ele}^{-1}, equivalent to the average level of conventional geothermal power plants. However, the system will be converted into a stable, flexible, controllable, and reliable carbon-free power source supplying the demand of the facilities and applications nearby, helping balance the intermittency of other renewable sources in the microgrid or act as a peak power plant in a large utility grid. As a reference, the LCOE of using utility-scale batteries (assuming a lifetime of 10 years) after the generators as the energy storage is also evaluated. Although the electricity production can also be stable and controllable, the overall electricity production capacity will remain the same as the system without energy storage (around 3/4 of the design point). The LCOE of using utility-scale batteries will be increased to 0.172 USD_{2020} kWh_{ele}^{-1}, which is equivalant to the upper limit of the LCOE range of conventional geothermal power plants. Moreover, compared to the battery, by allowing the ORC system to constantly operate under its optimum working conditions, the CTES can reduce the maintenance costs, reduce the frequency of working fluid replacement, and increase the lifetime of the ORC components, which are worth exploring in future studies.

The PBP, on the other hand, is sensitive to the electricity price. Without energy storage, the system can only supply the baseload in the power market. Due to the low price of the baseload service, the PBP of the AEW-ORC system without energy storage can be more than 30 years. Penalties of the power markets for not fulfilling the power generation tasks can further reduce the profit and increase the PBP. With energy storage, the system can be converted into a virtual powerplant or a demand response (DR) plant. Participating in the trading in a power market as a spinning contingency reserve, regulation reserve, or participating in retail DR programs together with the nearby users will bring extra profit to an energy storage equipped AEW-ORC system, since the electricity selling price can be significantly higher than supplying the baseload. For example, the critical peak rebate of a DR program in the US is 1.39 USD_{2020} kWh_{ele}^{-1}, which is ten times the average electricity price [34]. Even operating partially under this high price, the PBP can be significantly reduced. As shown in Fig. 18, if the average price can be above 0.25 USD_{2020} kWh_{ele}^{-1}, the PBP for CTES equipped AEW-ORC system will be less than 10 years. On the other hand, the PBP of the system with the battery is considerably higher than CTES. Therefore, CTES offers a more cost-effective energy storage solution to covert an AEW-ORC system into a stable and controllable power source.

4. Conclusions

In the present work, we proposed an innovative system integrating the utilization of abandoned exploitation wells (AEW), considering the horizontal extension and satellite LNG stations with thermal energy storage. The output temperatures of the AEW based geothermal system under the impact of several factors were systematically evaluated. The role of cold thermal energy storage (CTES) during the off-design operation is also assessed. The following conclusions can be derived:

Considering the horizontal extension and improving the thermal conductivity of the cement layer can both lead to a remarkable temperature increase in the recovered working fluid. Though an increase of horizontal extension can derive a temperature increment, the associated rate of increase would decline with the increase of the length.

Under the parameter scope of four impact factors set in the present study, the temperature of recovered working fluid is the most sensitive to the formation temperature gradient and depth of the vertical well, followed by the injection velocity of working fluid and length of the horizontal extension. Formation with a temperature gradient less than 0.03 K m^{-1} or AEW with a vertical well less than 4000 m is not recommended to use the current heat extraction and energy storage system design if the temperature requirement of the recovered fluid is above 90 ℃ to supply district heating.

Thanks to the LNG regasification process as the cold sink of the ORC, the power generation efficiencies are more than 20% for various AEW parameters and working conditions, considerably higher than the systems without the cold sink. However, the LNG demand profile fluctuation significantly reduces the average ORC efficiency and electrical power production by around one-third and one-fourth.

The designed CTES modules can increase the average ORC efficiency by 31.8% and the net electricity output by 25.0% during off-design operation. The LCOE of the AEW-ORC system without the energy storage is 0.092 USD_{2020} kW_{ele}^{-1}, lower than the range of conventional geothermal plants, indicating using AEW can significantly reduce the LCOE of geothermal power generation by saving the drilling cost. However, the power production is intermittent and unstable. With CTES, the LCOE will increase to 0.139 USD_{2020} kW_{ele}^{-1}, which is equivalent to the average levels of conventional geothermal plants. The stable power output with CTES enables the zero-emission geothermal and waste cold energy-based system as a possible source for peak load shifting and

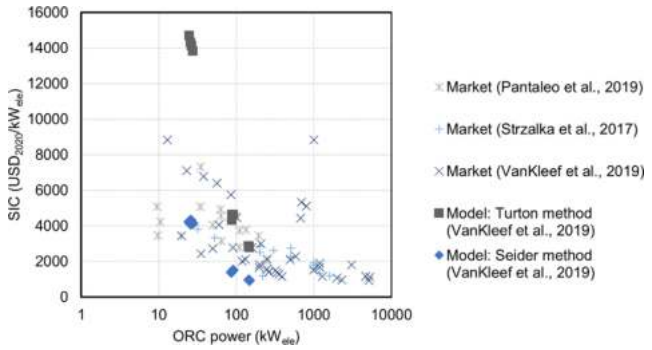

Fig. A1. SIC data for ORC cycles from market survey and model estimation.

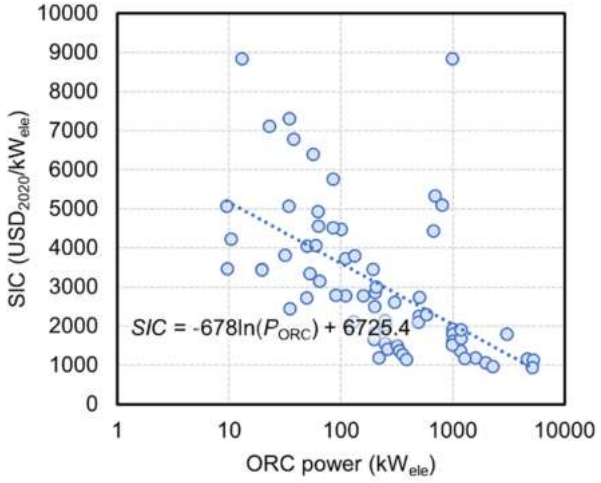

Fig. A2. SIC data for ORC cycles from the market surveys and logarithm regression as the estimate for the average.

virtual power plant that enjoys much higher electricity prices. In this case, the payback period can be significantly shorter than the AEW-ORC without CTES.

Future studies can focus on developing accurate economic models for the AEW heat extraction, especially for the investment cost. Based on that, an overall techno-economic analysis or life cycle analysis can be carried out, and the design optimization of the system can therefore be conducted using more economical and environmental merits. The ORC system efficiency can be further optimized by using better turbines and pumps, as well as adopting binary working fluids. Designing specific and smart control strategies for this application is also worth investigating. Moreover, while this study focuses on the power production using existing and planned collocated AEWs and satellite LNG stations, future work can also explore the other cold sinks if satellite LNG stations are not available near the AEWs, and study the impact of the distance between the heat and cold sources on the LCOE and PBP of the system.

Declaration of Competing Interest

The authors declare that they have no known competing financial interests or personal relationships that could have appeared to influence the work reported in this paper.

Acknowledgment

The authors want to thank Dr. Alessio Tafone, Dr. Jun Onn Khor (Nanyang Technological University), Dr. Baichang Wang (PetroChina Company Limited), Dr. Xiaojie Lin (Zhejiang University), Dr. Cheng Huang (Shanghai Xinghong Technology Co. Ltd), and Dr. Bo Wang (National University of Singapore) for their support in the information of abandoned exploitation wells, ORC systems, and district heating.

This work received financial support from the "Start-up Funding for New Faculty" provided by the Nanjing University of Aeronautics and Astronautics.

This study is also supported under the RIE2020 Industry Alignment Fund – Industry Collaboration Projects (IAF-ICP) Funding Initiative, as well as cash and in-kind contributions from Surbana Jurong Pte Ltd.

This research is partially funded by the Ministerio de Ciencia Innovación y Universidades de España (RTI2018-093849-B-C31—MCIU/AEI/FEDER, UE), and the Ministerio de Ciencia, Innovación y Universidades—Agencia Estatal de Investigación (AEI) (RED2018-102431-T). This work is partially supported by ICREA under the ICREA Academia program. The authors at the University of Lleida would like to thank the Catalan Government for the quality accreditation given to their research group (2017 SGR 1537). GREiA is a certified agent TECNIO in the category of technology developers from the Government of Catalonia.

Appendix A

Estimation for the ORC specific investment costs

The specific investment costs from various market surveys and model estimations are plotted in Fig. A.1. As can be seen clearly, for the power range from 20 to 100 kW_{ele}, the market data from various sources collected in different years keep a good consistency. However, the model estimations significantly deviate from the average market data. The Turton model tends to overestimate the SIC. Especially for power ranges below 50 kW_{ele}, the SIC will be significantly higher than the average market values. The Seider model, on the other hand, tends to underestimate the SIC, especially for the power range above 50 kW_{ele}.

Therefore, since the power of the ORC system in this study is between 20 and 100 kW_{ele}, it is better to use the average market data (as shown in the regression line of Fig. A.2) for the estimation of the ORC investment costs.

References

[1] M (2009). M Thermal Management Fluids: Cool Under Fire - Dielectric heat transfer fluid solutions for military and aerospace applications.
[2] N. Abas, A.R. Kalair, N. Khan, A. Haider, Z. Saleem, M.S. Saleem, Natural and synthetic refrigerants, global warming: a review, Renew. Sustain. Energy Rev. 90 (2018) 557–569.
[3] S. Acha, C. Hernandez-Aramburo, Integrated modelling of gas and electricity distribution networks with a high penetration of embedded generation, 2008.
[4] S. Akar, C. Augustine, P. Kurup, Global value chain and manufacturing analysis on geothermal power plant turbines. Thermodynamic Analysis and Optimization of Geothermal Power Plants, Elsevier, 2021, pp. 17-41.
[5] E. Allison, B. Mandler, Abandoned Wells: What happens to oil and gas wells when they are no longer productive? Petroleum and the Environment, American Geoscience Institute (AGI)., 2018, 7.
[6] J.Z. Alvi, Y. Feng, Q. Wang, M. Imran, L.A. Khan, G. Pei, Effect of phase change material storage on the dynamic performance of a direct vapor generation solar organic rankine cycle system, Energies 13 (22) (2020) 5904.
[7] S.A. Andersen, J.M. Conlin, K. Fjeldgaard, S.A. Hansen, Exploiting reservoirs with horizontal wells: the maersk experience, Oilfield Review; (Netherlands) 2 (3) (1990).
[8] ARA, 2022 China Natural Gas Pipeline Map. Retrieved 12 April, 2022, 2022, from http://chinagasmap.com/aboutthismap/segmentmarkets/chinagaspipelinemap.htm.
[9] I.H. Bell, J. Wronski, S. Quoilin, V. Lemort, Pure and pseudo-pure fluid thermophysical property evaluation and the open-source thermophysical property library CoolProp, Ind. Eng. Chem. Res. 53 (6) (2014) 2498–2508.
[10] Bitzer, S. E. Complete refrigerant data.
[11] J. Blank, K. Deb, pymoo: Multi-objective optimization in python, IEEE Access 8 (2020) 89497–89509.
[12] Q. Blondel, N. Tauveron, N. Caney, N. Voeltzel, Experimental study and optimization of the Organic Rankine Cycle with pure NovecTM649 and zeotropic mixture NovecTM649/HFE7000 as working fluid, Appl. Sci. 9 (9) (2019) 1865.
[13] X. Bu, W. Ma, H. Li, Geothermal energy production utilizing abandoned oil and gas wells, Renew. Energy 41 (2012) 80–85.

[14] M.A. Chatzopoulou, M. Simpson, P. Sapin, C.N. Markides, Off-design optimisation of organic Rankine cycle (ORC) engines with piston expanders for medium-scale combined heat and power applications, Appl. Energy 238 (2019) 1211–1236.
[15] K. Chen, Y. Du, Y. Yang, Y. Dai, J. Wang, P. Zhao, A comprehensive geothermal system in the usage of oilfield associated water from abandoned oil wells.
[16] K. Chen, H. Yu, G. Fan, Y. Zhang, Y. Dai, Multi-objective optimization of a novel combined parallel power generation system using CO2 and N2 for cascade recovery of LNG cryogenic energy, Energy Convers. Manage. 256 (2022), 115395.
[17] Y. Chen, Physical Fluid Dynamics, China Science and Technology Press, Hefei, 2008.
[18] W.-L. Cheng, Y.-H. Huang, D.-T. Lu, H.-R. Yin, A novel analytical transient heat-conduction time function for heat transfer in steam injection wells considering the wellbore heat capacity, Energy 36 (7) (2011) 4080–4088.
[19] W.-L. Cheng, T.-T. Li, Y.-L. Nian, C.-L. Wang, Studies on geothermal power generation using abandoned oil wells, Energy 59 (2013) 248–254.
[20] W.-L. Cheng, T.-T. Li, Y.-L. Nian, K. Xie, An analysis of insulation of abandoned oil wells reused for geothermal power generation, Energy Procedia 61 (2014) 607–610.
[21] W.-L. Cheng, T.-T. Li, Y.-L. Nian, K. Xie, Evaluation of working fluids for geothermal power generation from abandoned oil wells, Appl. Energy 118 (2014) 238–245.
[22] V. Chrz, C. Emmer, LNG directly to customer stations, Chart Ferox, Barcelona, 2007.
[23] W. Cole, A.W. Frazier, C. Augustine, Cost Projections for Utility-Scale Battery Storage: 2021 Update, National Renewable Energy Laboratory, Golden, CO. NREL/TP-6A20-79236, 2021.
[24] M. Collins, R. Law, The development and deployment of deep geothermal single well (DGSW) technology in the United Kingdom, Eur. Geol. J. 43 (2017) 63–68.
[25] A.P. Davis, E.E. Michaelides, Geothermal power production from abandoned oil wells, Energy 34 (7) (2009) 866–872.
[26] S. Detrow, Perilous Pathways: Behind The Staggering Number Of Abandoned Wells In Pennsylvania. Energy. Environment. Economy, 2021.
[27] ERIA, LNG Supply Chain Infrastructure Configuration. Formulating Policy Options for Promoting Natural Gas Utilization in the East Asia Summit Region. U. T. and I. K. Jakarta: ERIA. II, 2008, 9-22.
[28] FEMP, 2020 Discount Rates. U. S. D. o. Energy. Washington DC, Energy.GOV, 2020.
[29] H. Gadd, S. Werner, Achieving low return temperatures from district heating substations, Appl. Energy 136 (2014) 59–67.
[30] Gehringer, M. and V. Loksha (2012). Geothermal Handbook: Planning and Financing Power Generation A Pre-launch.
[31] N. Groom, Millions of abandoned oil wells are leaking methane, a climate menace, Commodities News, Salyersville, Kentucky, Reuters, 2020.
[32] Y. Guo, H. Wang, J. Lian, Review of integrated installation technologies for offshore wind turbines: Current progress and future development trends, Energy Convers. Manage. 255 (2022), 115319.
[33] S.E. Haaland, Simple and explicit formulas for the friction factor in turbulent pipe flow, J. Fluids Eng. 105 (1) (1983) 89–90.
[34] E.T. Hale, L.A. Bird, R. Padmanabhan, C.M. Volpi, Potential roles for demand response in high-growth electric systems with increasing shares of renewable generation, National Renewable Energy Lab.(NREL), Golden, CO (United States), 2018.
[35] L. He, Industrialization application and thought of Ningbo LNG cold energy air separation, Chemical Industry 34 (2016) 18–22.
[36] L. He, Industrialization application and thought of Ningbo LNG cold energy air separation, Chem Industry 34 (3) (2016) 18–22.
[37] D. Hu, S. Li, Y. Zheng, J. Wang, Y. Dai, Preliminary design and off-design performance analysis of an Organic Rankine Cycle for geothermal sources, Energy Convers. Manage. 96 (2015) 175–187.
[38] D. Hu, Y. Zheng, Y. Wu, S. Li, Y. Dai, Off-design performance comparison of an organic Rankine cycle under different control strategies, Appl. Energy 156 (2015) 268–279.
[39] IRENA, Renewable Power Generation Costs in 2017. International Renewable Energy Agency, Abu Dhabi, 2018.
[40] IRNEA (2021). Renewable Power Generation Costs in 2020.
[41] A.N. Johnson, W. Johansen, Comparison of Five Natural Gas Equations of State Used for Flow and Energy Measurement, 2009.
[42] S. Joshi, Cost/benefits of horizontal wells. SPE western regional/AAPG Pacific section joint meeting, OnePetro, 2003.
[43] M. Kang, S. Christian, M.A. Celia, D.L. Mauzerall, M. Bill, A.R. Miller, Y. Chen, M. E. Conrad, T.H. Darrah, R.B. Jackson, Identification and characterization of high methane-emitting abandoned oil and gas wells, Proc. Natl. Acad. Sci. 113 (48) (2016) 13636–13641.
[44] S.H. Kang, Design and experimental study of ORC (organic Rankine cycle) and radial turbine using R245fa working fluid, Energy 41 (1) (2012) 514–524.
[45] A. Kant, Oilfield abandonment and soil restoration in the netherlands, experiences for the future. SPE International Conference on Health, Safety and Environment in Oil and Gas Exploration and Production, OnePetro, 2010.
[46] J.C. Kurnia, M.S. Shatri, Z.A. Putra, J. Zaini, W. Caesarendra, A.P. Sasmito, Geothermal energy extraction using abandoned oil and gas wells: Techno-economic and policy review, Int. J. Energy Res. 46 (1) (2022) 28–60.
[47] Legal-Graphics, Oil & Gas. Graphic Design 3 Retrieved 31 August, 2021, 2021, from https://legalgraphics.net/graphic-design/oil-gas/.
[48] E.W. Lemmon, M.L. Huber, M.O. Mclinden, NIST standard reference database 23: reference fluid thermodynamic and transport properties-REFPROP, version 8.0., 2007.
[49] M. Macenić, T. Kurevija, Revitalization of abandoned oil and gas wells for a geothermal heat exploitation by means of closed circulation: Case study of the deep dry well Pčelić-1, Interpretation 6 (1) (2018) SB1-SB9.
[50] M.M. Marsh, New brunswick onshore oil and natural gas well abandonment study, Petroleum Research Atlantic Canada (PRAC) 1 (8) (2004) 15.
[51] C. Maxwell, Cost Indices, 2020. Retrieved 22 April, 2022, from https://www.toweringskills.com/financial-analysis/cost-indices/.
[52] V. Mehdikhani, I. Mirzaee, M. Khalilian, M. Abdolalipouradl, Thermodynamic and exergoeconomic assessment of a new combined power, natural gas, and hydrogen system based on two geothermal wells, Appl. Therm. Eng. 206 (2022), 118116.
[53] J.R. Mehrenjani, A. Gharehghani, A.G. Sangesaraki, Machine learning optimization of a novel geothermal driven system with LNG heat sink for hydrogen production and liquefaction, Energy Convers. Manage. 254 (2022), 115266.
[54] A. Mosaffa, N.H. Mokarram, L.G. Farshi, Thermo-economic analysis of combined different ORCs geothermal power plants and LNG cold energy, Geothermics 65 (2017) 113–125.
[55] Y.-L. Nian, W.-L. Cheng, Evaluation of geothermal heating from abandoned oil wells, Energy 142 (2018) 592–607.
[56] Y.-L. Nian, W.-L. Cheng, Insights into geothermal utilization of abandoned oil and gas wells, Renew. Sustain. Energy Rev. 87 (2018) 44–60.
[57] K. Ojukwu, Managing abandonment issues in Nigerian oil & gas Industry. KI Ojukwu,“ Managing Abandonment Issues in Nigerian Oil & Gas Industry”(OGEL, ISSN 1875-418X) August., 2020.
[58] A. Pantaleo, M. Simpson, G. Rotolo, E. Distaso, O. Oyewunmi, P. Sapin, P. De Palma, C. Markides, Thermoeconomic optimisation of small-scale organic Rankine cycle systems based on screw vs. piston expander maps in waste heat recovery applications, Energy Convers. Manage. 200 (2019), 112053.
[59] A.E. Prasetya, R. Rakhmahwidiati, R.D. Hutabarat, Plug and abandonment procedures for onshore wells and the utilization of reserved abandonment and site restoration ASR funds, SPE Symposium: Decommissioning and Abandonment. Day 1 Mon, December 03, 2018.
[60] S. Quoilin, M.V.D. Broek, S. Declaye, P. Dewallef, V. Lemort, Techno-economic survey of Organic Rankine Cycle (ORC) systems, Renew. Sustain. Energy Rev. 22 (2013) 168–186.
[61] S. Quoilin, S. Declaye, B.F. Tchanche, V. Lemort, Thermo-economic optimization of waste heat recovery Organic Rankine Cycles, Appl. Therm. Eng. 31 (14) (2011) 2885–2893.
[62] D. Raimi, A.J. Krupnick, J.-S. Shah, A. Thompson, Decommissioning orphaned and abandoned oil and gas wells: new estimates and cost drivers, Environ. Sci. Technol. 55 (15) (2021) 10224–10230.
[63] H.J. Ramey Jr., Wellbore heat transmission, J. Petrol. Technol. 14 (04) (1962) 427–435.
[64] D. Ravikumar, G.A. Keoleian, S.A. Miller, V. Sick, Assessing the Relative Climate Impact of Carbon Utilization for Concrete, Chemical, and Mineral Production. Environmental Science & Technology 55(NREL/JA-6A20-81074, 2021; MainId: 79850;UUID:a77f9bae-1d5a-4dfa-af13-233cf10115eb;MainAdminID:63023): Medium: X.
[65] J. Ren, L. Zhang, S. Ren, J. Lin, S. Meng, G. Ren, T. Gentzis, Multi-branched horizontal wells for coalbed methane production: field performance and well structure analysis, Int. J. Coal Geol. 131 (2014) 52–64.
[66] R.M. Rial, 3D Thermal Simulation Using a Horizontal Wellbore for Steamflooding. SPE Annual Technical Conference and Exhibition. All Days, 1984.
[67] scikit-optimize-Contributors (2021). scikit-optimize Documentation.
[68] W.D. Seider, J.D. Seader, D.R. Lewin, S. Widagdo, Product and Process Design Principles - Synthesis, Analysis, and Evaluation, John Wiley & Sons Inc., New York, 2009.
[69] R. Smith, Chemical Process Design and Integration. United Kingdom, John Wiley & Sons Ltd., 2005.
[70] P.L. Solutions, G. Gardner, Inactive Oil and Gas Wells on Federal Lands and Minerals: Potential Costs and Conflicts, 2021.
[71] J. Song, P. Loo, J. Teo, C.N. Markides, Thermo-economic optimization of organic Rankine cycle (ORC) systems for geothermal power generation: a comparative study of system configurations, Front. Energy Res. 8 (2020) 6.
[72] Srinivasan, S., J.M. Joshi, J.L. Narasimham, M. Rao, S. Barua, K.N. Jha, Feasibility of Development of Marginal Fields Through Horizontal Well Technology. SPE/DOE Improved Oil Recovery Symposium. All Days, 1996.
[73] R. Strzalka, D. Schneider, U. Eicker, Current status of bioenergy technologies in Germany, Renew. Sustain. Energy Rev. 72 (2017) 801–820.
[74] N. Tay, M. Belusko, F. Bruno, An effectiveness-NTU technique for characterising tube-in-tank phase change thermal energy storage systems, Appl. Energy 91 (1) (2012) 309–319.
[75] TESLAB@NTU, 2022. THERMAL ENERGY SYSTEMS LAB. Retrieved May 27, 2022, from https://www.thermalenergysystemslab.com/.
[76] Z. Tian, Y. Yue, Y. Zhang, B. Gu, W. Gao, Multi-objective thermo-economic optimization of a Combined Organic Rankine Cycle (ORC) system based on waste heat of dual fuel marine engine and LNG cold energy recovery, Energies 13 (6) (2020) 1397.
[77] Tractebel-Engineering (2015). Mini and Micro LNG for Commercialization of Small Volumes of Associated Gas. World Bank, Washington, DC. © World Bank.
[78] UNITROVE. (2021). Unitrove Natural Gas Calorific Value Calculator Retrieved Nov 20, 2021, from https://www.unitrove.com/engineering/tools/gas/natural-gas-calorific-value.
[79] L.M. van Kleef, O.A. Oyewunmi, C.N. Markides, Multi-objective thermo-economic optimization of organic Rankine cycle (ORC) power systems in waste-heat recovery applications using computer-aided molecular design techniques, Appl. Energy 251 (2019), 112513.

[80] J. Wang, J. Wang, Y. Dai, P. Zhao, Thermodynamic analysis and optimization of a transcritical CO2 geothermal power generation system based on the cold energy utilization of LNG, Appl. Therm. Eng. 70 (1) (2014) 531–540.
[81] G.P. Willhite, Over-all heat transfer coefficients in steam and hot water injection wells, J. Petrol. Technol. 19 (05) (1967) 607–615.
[82] Z. Wu, New energy and renewable energy utilization, Mechanical Industrial Press, Beijing, 2006.
[83] G. Xu, S.-W. Wong, Interaction of multiple non-planar hydraulic fractures in horizontal wells. International Petroleum Technology Conference, 2013.
[84] W.-D. Xu, H.-J. Bian, S.-S. Fan, B. Hua, Research on cold energy utilization techniques at LNG satellite stations [J], Nat. Gas. Ind. (2009) 5.
[85] L. Yang, A. Gil, P.S.H. Leong, J.O. Khor, B. Akhmetov, W.L. Tan, S. Rajoo, L. F. Cabeza, A. Romagnoli, Bayesian optimization for effective thermal conductivity measurement of thermal energy storage: An experimental and numerical approach, J. Storage Mater. 52 (2022), 104795.
[86] L. Yang, U. Villalobos, B. Akhmetov, A. Gil, J.O. Khor, A. Palacios, Y. Li, Y. Ding, L. F. Cabeza, W.L. Tan, A comprehensive review on sub-zero temperature cold thermal energy storage materials, technologies, and applications: State of the art and recent developments, Appl. Energy 116555 (2021).
[87] L. Yang, U. Villalobos, B. Akhmetov, J.O. Khor, A. Gil, W.L. Tan, A. Romagnoli, 2021. Editor(s): Luisa F. Cabeza, Encyclopedia of Energy Storage, Elsevier, 2022, Pages 479-497, ISBN 9780128197301, https://doi.org/10.1016/B978-0-12-819723-3.00029-9 (https://www.sciencedirect.com/science/article/pii/B9780128197233000299).
[88] L. Yang, H. Xu, F. Cola, B. Akhmetov, A. Gil, L.F. Cabeza, A. Romagnoli, Shell-and-tube latent heat thermal energy storage design methodology with material selection, storage performance evaluation, and cost minimization, Applied Sciences 11 (9) (2021) 4180.
[89] Y. Yang, Y. Huo, W. Xia, X. Wang, P. Zhao, Y. Dai, Construction and preliminary test of a geothermal ORC system using geothermal resource from abandoned oil wells in the Huabei oilfield of China, Energy 140 (2017) 633–645.
[90] M.A. Emadi, J. Mahmoudimehr, Modeling and thermo-economic optimization of a new multi-generation system with geothermal heat source and LNG heat sink, Energy Convers. Manage. 189 (2019) 153–166, https://doi.org/10.1016/j.enconman.2019.03.086.